

Blue Lurkers: Hidden Blue Stragglers on the M67 Main Sequence Identified from Their Kepler/K2 Rotation Periods

Emily Leiner 1,2,7 , Robert D. Mathieu 6, Andrew Vanderburg 8,8 , Natalie M. Gosnell 6, and Jeffrey C. Smith 6,6
Center for Interdisciplinary Exploration and Research in Astrophysics, Northwestern University, 2145 Sheridan Rd., Evanston, IL 60208, USA emily.leiner@northwestern.edu

Department of Astronomy, University of Wisconsin-Madison, 475 North Charter St., Madison, WI 53706, USA Department of Astronomy, University of Texas at Austin, Austin, TX 78712 USA Department of Physics, Colorado College, 14 E. Cache La Poudre St., Colorado Springs, CO 80903, USA SETI Institute, Mountain View, CA 94043, USA NASA Ames Research Center, Moffett Field, CA 94035, USA Received 2019 March 31; revised 2019 June 13; accepted 2019 June 21; published 2019 August 12

Abstract

At an age of 4 Gyr, typical solar-type stars in M67 have rotation rates of 20–30 days. Using K2 Campaign 5 and 16 light curves and the spectral archive of the WIYN Open Cluster Study, we identify 11 3D kinematic members of M67 with anomalously fast rotation periods of 2–8 days, implying ages of less than 1 Gyr. We hypothesize that these anomalously fast rotators have been spun up by mass transfer, mergers, or stellar collisions during dynamical encounters within the 1 Gyr and thus represent lower-luminosity counterparts to the blue straggler stars. These 11 candidate post-interaction stellar systems have much in common with the blue stragglers, including a high binary fraction (73%); a number of long-period, low-eccentricity binary systems; and in at least one case a UV excess consistent with the presence of a hot white dwarf companion. The identification of these 11 systems provides the first picture of the low-luminosity end of the blue straggler distribution, providing new constraints for detailed binary evolution models and cluster population studies. This result also clearly demonstrates the need to properly account for the impact of binaries on stellar evolution, as significant numbers of post-interaction binaries likely exist on cluster main sequences and in the field. These stars are not always easy to identify but make up $\sim 10\%$ or more of the spectroscopic binary population among the solar-type stars in M67.

Key words: binaries: spectroscopic – blue stragglers – open clusters and associations: individual (M67) – stars: rotation – stars: solar-type

1. Introduction

In color–magnitude diagrams (CMDs) of star clusters, blue straggler stars (BSSs) are found brighter and bluer than the main-sequence (MS) turnoff. BSSs are thought to form from mass transfer in binary systems (McCrea 1964; Gosnell et al. 2014), stellar collisions during dynamical encounters (Leonard 1989; Sills et al. 2001), or binary mergers (e.g., induced by Kozai cycles; Ivanova et al. 2008; Perets & Fabrycky 2009).

BSSs are not the only mass transfer, merger, or collision products that exist in clusters. Evolved counterparts to the BSSs (sometimes called "yellow giants" or "yellow stragglers") are observed in between the BSS region and the red giant branch or detected as overmassive cluster giants via asteroseismology (Landsman et al. 1997; Corsaro et al. 2012; Leiner et al. 2016; Handberg et al. 2017).

In principle, lower-mass BSSs could form via mass accretion onto initially lower-mass secondaries, through less efficient mass transfer processes, or via mergers or collisions of two lower-mass MS stars. Such lower-mass BSSs would be hidden within cluster MSs because their new luminosities would not be high enough to appear above the turnoff in the cluster CMD as the classical BSSs do. Indeed, *N*-body and population synthesis studies predict that such mass transfer or merger products may be numerous (Andronov et al. 2006; Geller et al. 2013).

Actually detecting these low-mass BSSs on the MS is challenging. Very close MS-white dwarf (WD) binaries can be detected in time-series photometric surveys if they are eclipsing (e.g., Almenara et al. 2012; Breton et al. 2012; Parsons et al. 2015), or from X-ray and transient surveys in cases where there is active accretion and/or outbursts such as novae and cataclysmic variables (e.g., Strope et al. 2010; Szkody et al. 2011; Fornasini et al. 2014). Post-mass-transfer binaries in wider orbits (P > 10 days) with hot WD companions can also be identified in UV surveys (e.g., Jeffries & Stevens 1996; Rebassa-Mansergas et al. 2010, 2017; Gosnell et al. 2014; Li et al. 2014; Parsons et al. 2016; van Roestel et al. 2018), but older post-mass-transfer systems with fainter, cooler WD companions escape detection in these studies, as do merger and collision products. As a result, the full extent of the postinteraction MS population of clusters is not known. A better census of the post-interaction population requires developing other techniques that may be used to identify these postinteraction stars that blend photometrically with cluster MS stars.

One method is using stellar abundance measurements. Stellar merger and mass transfer products are predicted to have spectral signatures including barium, carbon, oxygen, or lithium abundance anomalies. This technique has identified many BSS counterparts in the field such as carbon-enhanced metal-poor stars with *s*-process enrichment (CEMP-*s* stars), barium stars, and lithium-enhanced giants (e.g., Jorissen et al. 1998; Aoki et al. 2008; Hansen et al. 2016). Detecting these post-interaction systems from abundance signatures requires

⁷ NSF Astronomy & Astrophysics Fellow.

⁸ NASA Sagan Fellow.

high-resolution spectra, and known BSSs do not always have the observed abundance signatures expected from mass transfer or collisional formation (Shetrone & Sandquist 2000; Milliman et al. 2016). The observational biases and completeness of abundance detection methods are not well defined.

Here we propose an alternative technique to identify recent mass transfer and collision products, using rotation rates. Recent advances in our understanding of stellar angular momentum evolution have revealed a clearer picture of the rotational evolution of solar-like stars. Observations of young clusters show that on the pre-MS these stars have a wide range of rotation periods. Early in their lives these stars spin down owing to magnetic braking (e.g., via a magnetized wind or disk locking; Matt & Pudritz 2005; Gallet & Bouvier 2013), with faster rotators spinning down more quickly as a result of their stronger magnetic fields.

After several hundred Myr, solar-type stars of the same age will converge to the same rotation rate regardless of their initial angular momentum (e.g., Barnes 2003; Gallet & Bouvier 2013; Epstein & Pinsonneault 2014; Meibom et al. 2009, 2015). Thereafter stellar rotation rates can be used as a proxy for stellar age, a technique known as gyrochronology. Recently, Leiner et al. (2018) have suggested that the same gyrochronology age determinations may also be used in post-mass-transfer systems.

Given the wealth of observational and theoretical evidence (Section 2), we presume that anomalously rapid rotation rates are observed among all stars that have recently undergone a merger, collision, or mass transfer event. Therefore, rotation rates from spectroscopic $v \sin i$ measurements or photometric spot modulation may be an effective way to select for recent stellar interaction products.

As a test case, we look at stellar rotation rates among stars in the old (4 Gyr) open cluster M67, looking for any MS cluster members with rotation periods much shorter than the 20–30 days measured for MS stars in the cluster (Barnes et al. 2016; Gonzalez 2016). This study is the first to use rotation to identify the post-interaction population of a cluster and offers the first glimpse of the low-luminosity end of the BSS distribution.

In Section 2 we discuss our premise that rapid rotation is a sign of mass transfer, merger, or collision formation. In Section 3 we discuss the *K*2 observations of M67 and our technique for light-curve extraction and analysis. In Section 4 we discuss each of our candidate post-interaction systems in detail. In Section 5 we discuss the overall population characteristics of the anomalously rapid rotators in the cluster that we suggest formed from recent mass transfer or collision events. In Section 6 we discuss the significance of these detections and summarize our results.

2. The Rotational Evolution of Mass Transfer Products

In theory, mass transfer in a binary also transports significant angular momentum, resulting in substantial spin-up of the mass-accreting star (Packet 1981; de Mink et al. 2013). Similarly, stellar collisions are expected to yield rapidly rotating stellar products (Sills et al. 2002, 2005). These interactions, then, can be seen as resetting the gyro-age clock, giving old stars the rapid rotation rates indicative of youth.

Observations confirm that many mass transfer and collision products like the BSSs are rotating rapidly (e.g., Jeffries & Stevens 1996; Carney et al. 2005; Lovisi et al. 2010; Mucciarelli et al. 2014; Nemec et al. 2017). These BSSs are sometimes observed to have $v \sin i$ measurements as large as $200 \, \mathrm{km \, s^{-1}}$. In previous work (Leiner et al. 2018), we provided the first observational study of spin-down in post-mass-transfer binaries. This work used a sample of 12 post-mass-transfer systems, all composed of an FGK MS star with a hot WD companion. The WDs in these systems had measured temperatures, and thus their ages (i.e., time since mass transfer ceased) could be determined from WD cooling. The FGK primaries also had measured rotation rates from either photometric spot modulation or spectroscopic $v \sin i$ values.

Comparing the WD cooling ages to measured rotation periods, Leiner et al. (2018) concluded that young (less than several Myr) post-mass-transfer systems have rotation periods <1 day, or 30%–40% of their critical rotation rate. Older systems have slower rotation rates, with the relationship following approximately the spin-down curves for normal solar-type stars from Gallet & Bouvier (2015). From this work, Leiner et al. (2018) concluded that rotation may be a useful indicator for age in post-mass-transfer systems in which WD ages are not available. Further, they suggested that gyrochronology relationships developed for normal FGK stars (i.e., Angus et al. 2015) may also be applicable to FGK post-mass-transfer binaries.

Another implication of this work is that rapid rotation rates may be indicative of a recent episode of mass transfer. In M67, typical MS rotation rates are 20–30 days (Barnes et al. 2016; Gonzalez 2016), except for systems in short-period binaries in which rotation has been tidally synchronized with the orbital period. Much shorter rotation periods, then, may be a way to select single stars and wide binary systems that have been through a recent interaction. Here we test this idea in M67, searching for anomalously rapid rotators in the cluster that may be post-interaction binaries formed in mass transfer, mergers, or collisions.

3. Observations

3.1. WIYN Open Cluster Study

M67 (NGC 2682) is a well-studied old (4 Gyr; Nissen et al. 1987; Montgomery et al. 1993; Stello et al. 2016) open cluster located at $\alpha = 8^{\rm h}51^{\rm m}23^{\rm s}$, $\delta = +11^{\circ}49'02''$ (J2000; Geller et al. 2015). Distance measurements for the cluster range from approximately 800 to 900 pc (Geller et al. 2015). Throughout this work we adopt a distance modulus of $(m-M)_0 =$ 9.70 ± 0.05 (Sarajedini et al. 2009) and a reddening of E(B-V) = 0.041 (Taylor 2007). M67 has extensive archival photometry (Montgomery et al. 1993; Fan et al. 1996; van den Berg et al. 2004), proper-motion memberships (Sanders 1977; Girard et al. 1989), and time-series radial-velocity measurements from more than 40 yr of high-precision radial velocities obtained on the WIYN 3.5 m telescope with the Hydra Multi-Object Spectrograph and with the Harvard-Smithsonian Center for Astrophysics Digital Speedometers. These radial-velocity data are stored in the archive of the WIYN Open Cluster Study (WOCS; Mathieu 2000). Geller et al. (2015) incorporate both proper motions and radial velocities to determine memberships and binary status for stars in the cluster field out to a radius of 30'. A subsequent paper will publish orbital solutions for the

⁹ We note that tidally synchronized binaries will be rotating faster than this. These stars are easily excluded from our sample as we explain in Section 3.3.

known binaries (A. M. Geller et al. 2019, in preparation). This WOCS synthesis contains members down to a limiting magnitude of V=16.5, a sample that includes BSSs, the subgiant and giant branches, and FGK MS stars. In our analysis, we adopt the most up-to-date membership information and binary orbital parameters from these WOCS papers.

For this study, we select only MS members of M67. We therefore exclude all stars from Geller et al. (2015) on the subgiant branch red of (B-V)=0.6 and on the red giant branch. We also exclude any stars they classify as BSSs. Specifically, Geller et al. (2015) identify 14 BSSs in M67 brighter than the MS turnoff. We note that this sample excludes a few BSS candidates from the literature that fall in a region just above or to the blue of the MS turnoff. Stars in these CMD regions are identified as BSSs by some authors, but their classification is not certain. They may be explained as the combined light of an MS binary system, or as evolving through the blue hook phase, in which case the expected temperature and luminosity are sensitive to detailed assumptions in the stellar evolution models. Following Geller et al. (2015), we classify these as MS stars for this work.

3.2. K2 Observations of M67

M67 was observed in Campaign 5 (K2 Guest Observer Program 5031; PI: Mathieu) of the Kepler¹⁰ space telescope's extended K2 mission for 76 continuous days between 2015 April 27 and July 10. Observations used a combination of individual apertures to target cluster members on the outskirts of the cluster and short-cadence targets and a 25' by 25' superstamp of pixels covering the cluster center in order to efficiently observe all stars in the cluster core. M67 was reobserved in Campaign 16 (2017 December 7-2018 February 25), providing an additional 81 days of time-series photometry for most of the cluster members observed in Campaign 5 in addition to light curves for some new sources not observed in the first campaign. For Campaigns 5 and 16, light curves for both the individual targets and the targets in the superstamp were extracted and corrected for K2 systematic errors using the CfA light-curve reduction pipeline K2SFF (Vanderburg & Johnson 2014; Vanderburg et al. 2016). As described in Vanderburg et al. (2016), light curves were extracted using 20 apertures, and the aperture with the highest photometric precision was selected for our analysis.

While these methods effectively remove systematics caused by the *K*2 6 hr pointing drift, they leave in long-term instrumental systematics that can impede searches for long-period signals like stellar rotation. To remove these systematics, we used the *Kepler* team's Pre-search Data Conditioning-Maximum A Posteriori (PDC-MAP) software (Smith et al. 2012; Stumpe et al. 2014) to identify and remove common-mode instrumental trends. Unlike the standard *Kepler* export data products, we utilized *single-scale* PDC-MAP, which performs best at removing long-term trends while preserving long-period signals. This process is described in more detail in Esselstein et al. (2018).

3.3. Rotation Measurements

We selected all 3D kinematic members or likely members of the M67 MS observed in K2 Campaign 5 or 16. For each star, we created a Lomb–Scargle periodogram using the light-curve

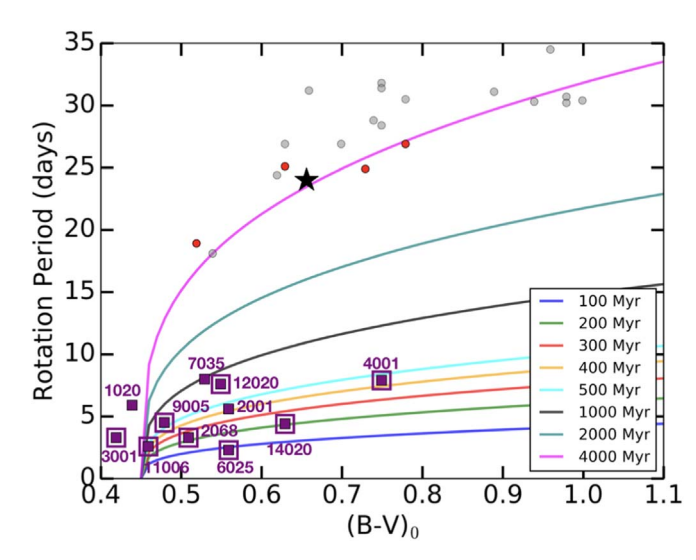


Figure 1. Color-rotation plot comparing the 11 rapid rotators in our sample (purple points) to a sample of normal M67 MS stars with rotation periods from Barnes et al. (2016; gray points). We highlight in red the Barnes et al. (2016) rotation periods that also have a measurement from the CfA and/or Oxford pipeline that agrees within 15%. Binaries are boxed as in Figure 2. All are dereddened using E(B-V) = 0.041 (Taylor 2007). For comparison, we also show gyrochronology models from Angus et al. (2015) for ages ranging from 100 Myr to 4 Gyr and the rotation rate of the Sun (black star).

processing software vartools (Hartman et al. 2008). As a first cut, we selected all stars from this sample with measured periods less than 15 days and power of at least 0.1. We crossreferenced these stars with the binary orbital information from WOCS (A. M. Geller et al. 2019, in preparation) to exclude any short-period binaries with orbital periods less than 60 days. We do this because tidal forces spin up the rotation rates of close binaries, confusing explanation of any observed rapid rotation. Among the \sim 2800 field eclipsing binaries in the Kepler Eclipsing Binary Catalog, Lurie et al. (2017) find that the fraction of tidally circularized binaries drops off at periods greater than 10 days, and the fraction of tidally synchronized binaries drops off dramatically at periods longer than 30 days. These cutoff periods are also compatible with tidal circularization studies in open clusters (Meibom & Mathieu 2005; Meibom et al. 2009). As a conservative cut, we double the Lurie et al. (2017) tidal synchronization limit, removing any binaries with $P_{\rm orb} < 60$ days from our sample.

We compare the remaining sample to the rotational models of Angus et al. (2015), selecting all stars with rotation rates faster than the 1 Gyr model (Figure 1). This age cut allows us to take into account the temperature of the star when determining whether rotation rates are unusual, as bluer stars close to the cluster turnoff naturally have slightly faster rotation rates than redder stars farther down the MS. These rotational models are undefined for stars hotter than $(B - V)_0 = 0.45$. There are a few stars in M67 blueward of this limit, and so for these hotter stars we use a rotation cut of $P_{\rm rot} < 8.0$ days, the approximate rotation rate of a 1 Gyr star near the cluster turnoff. For context, in Figure 1 we also show the rotation periods of a sample of normal MS stars in M67 from Barnes et al. (2016; gray points). These stars have rotation periods of \sim 25 days. We note that Esselstein et al. (2018) raise doubts about the reliability of many of the published M67 rotation periods, including those of Barnes et al. (2016). They find that for many sources different pipelines yield different rotation measurements. To highlight a

https://keplerscience.arc.nasa.gov

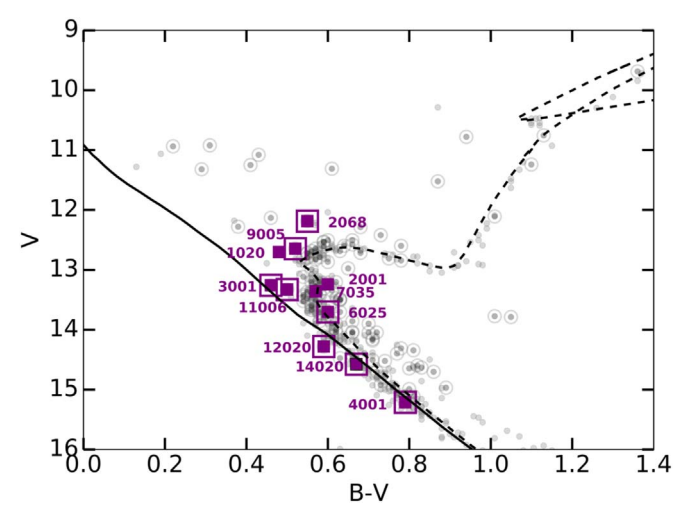


Figure 2. CMD showing 3D kinematic members of M67, with binary members boxed/circled (Geller et al. 2015). Purple points show stars with rapid rotation rates, which we suggest are products of recent stellar interactions. The black solid and dashed lines are the zero-age MS and a 4 Gyr PARSEC isochrone, respectively (Bressan et al. 2012). Both are reddened and shifted to the cluster distance.

more reliable sample, we show in red the rotation periods from Barnes et al. (2016) that also have a rotation measurement in Esselstein et al. (2018) that agrees within 15%. We also show the rotation period of the Sun, which is close in age to M67 stars.

For our sample of fast-rotating stars, we visually examine all the light curves and periodograms to remove any spurious or marginal results. We exclude some lower signal-to-noise ratio systems with multiple peaks. We check the light curves of each target's neighboring stars in the EPIC catalog¹¹ within 30" of each target to determine whether the observed periodic signals might originate with a nearby variable star. We also visually examine the CCD images from K2 to check for nearby stars and cross-reference with the Two Micron All Sky Survey (2MASS) catalog to check for any stars within 30" that may be missing from the EPIC database or too faint to identify in the images. In addition, we adjusted the size of the photometric aperture used to extract the light curve to check that the variability appears to be centered on these sources and does not become stronger with a larger aperture. Using these techniques, we remove several systems where the variability appears to originate with a neighboring star. These steps give us confidence that the remaining stars in our samples are true rotational variables.

We find nine stars in our sample that show rotation rates much faster than those of normal MS stars in M67. We show the CMD location of these stars in Figure 2. We also show raw light curves, phase-folded light curves, and Lomb–Scargle periodograms from both C5 and C16 for these nine stars in Figure 3. The measurement precision of these periods is generally good to a few percent for periods of several days, and up to 10%-20% for the longer 20-day periods or multiperiodic sources in our sample. We do not quote these measurement errors because for most of our sources they are misleadingly small. The more significant sources of error will be astrophysical, such as spot migration and differential rotation. We expect these to cause typical rotation period variations on the order of 10%, though in

some stars (with more extreme differential rotation, for example) it may be higher (Reinhold & Gizon 2015; Balona & Abedigamba 2016; Lurie et al. 2017).

As an additional independent check, we also compare these rotation periods to those produced using another light-curve production pipeline, the Oxford pipeline described by Esselstein et al. (2018) and Aigrain et al. (2015). For all sources, our measured periods agree with Esselstein period measurements from the Vanderburg light curves and with the Esselstein period measurements from the Oxford pipeline light curves (R. Esselstein 2019, private communication), though four sources (WOCS 2068, 1020, 7035, and 9005) do not meet their more conservative detection criteria (see Esselstein et al. 2018). We classify these detections as less certain and discuss these cases in more detail in the next section.

In addition, we measure $v \sin i$ rates for all 3D kinematic members of the cluster from Geller et al. (2015) (see Geller et al. 2008 for an explanation of our $v \sin i$ measurement technique), again excluding short-period binaries from our sample. The WOCS spectra have a v sin i measurement limit of 10 km s⁻¹. Typical stars in M67 with rotation rates of 20–30 days would be rotating with surface velocities well below this limit. We therefore consider any $v \sin i$ measurement above 10 km s⁻¹ to be an anomalously rapid rotator. We find that none of the nine stars discussed above have a $v \sin i >$ 10 km s⁻¹. This is not surprising since a rotational velocity of 10 km s⁻¹ corresponds to a 4-day rotation period for a turnoff star in the cluster. Given this detection limit, most of the stars in our sample would not have $v \sin i$ values above the WOCS velocity resolution limit regardless of inclination angle, and the rest would go undetected if the rotational axes of the systems are somewhat inclined.

We do, however, detect two additional stars with $v \sin i > 10 \, \mathrm{km \, s^{-1}}$, WOCS 3001 and 11006. These stars have $v \sin i$ measurements of 14.7 and 18.1 km s⁻¹, respectively. For these stars we convert $v \sin i$ to rotation period using the technique explained in Leiner et al. (2018). Briefly, we fit photometric radii to the CMD position of each star. Using this radius, we convert the observed rotational $v \sin i$ to a distribution of periods assuming a random, uniform distribution of inclinations. We adopt the median value of this period distribution as the rotation period and report the interquartile range of values as the uncertainty. Using this method, we derive rotation periods of $2.6^{3.4}_{1.4}$ days for WOCS 11006 and $3.3^{4.3}_{1.7}$ days for WOCS 3001.

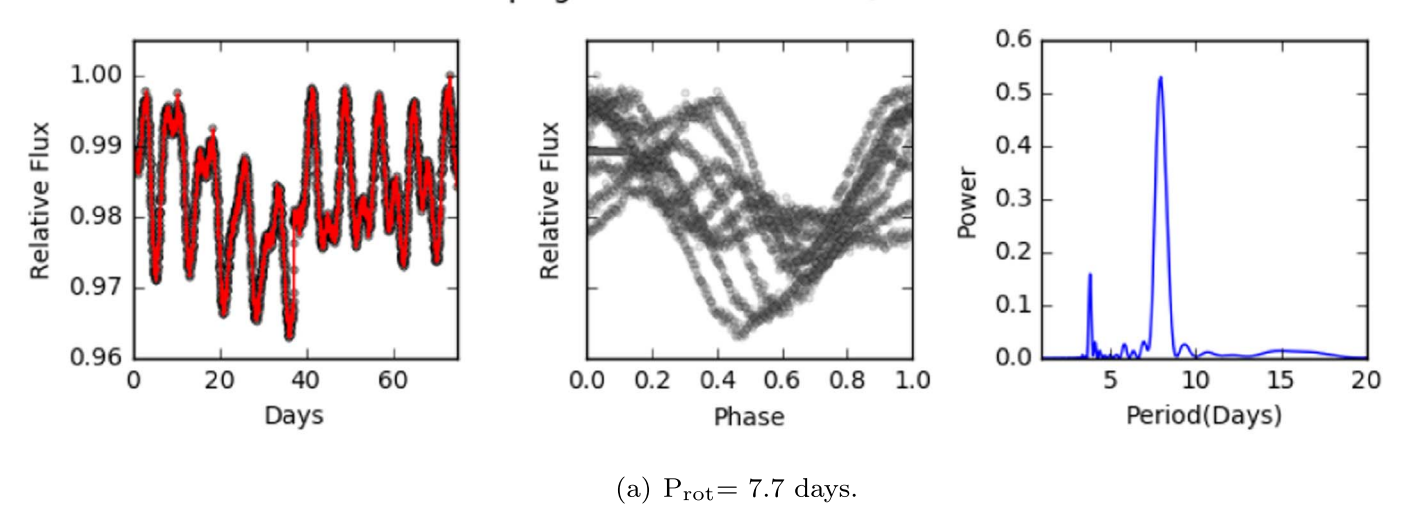
We adopt these values in Table 1, as these stars do not have well-measured photometric rotation periods. (We discuss this further in Section 4.) Despite the lack of a photometric signal, we consider both to be reliable detections and include these two systems in our sample using these spectroscopic rotation periods.

4. Discussion of Individual Stars

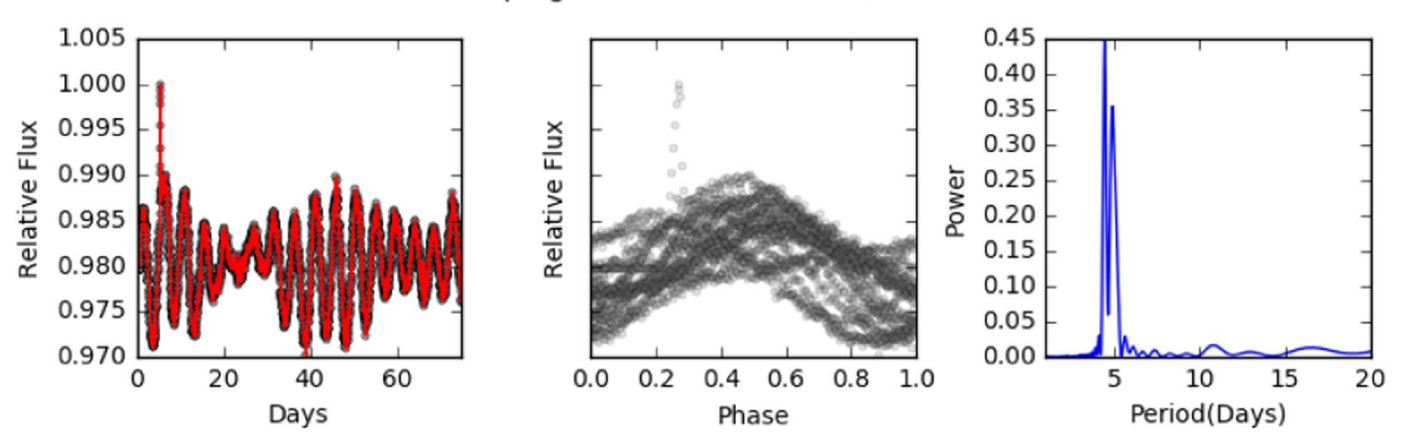
In Table 1 we list the stellar and orbital properties of the rapidly rotating MS stars. All these rapid rotators are high-probability proper-motion and radial-velocity members of M67. Nevertheless, there is a small probability that any individual star in our sample may be a field star whose 3D motion overlaps with the motion of the cluster. However, the probability that more than one of these stars is a field contaminant is negligible (Mathieu et al. 2003).

¹¹ https://archive.stsci.edu/k2/epic/search.php

Campaign 5 EPIC 211411716/WOCS 4001



Campaign 5 EPIC 211410278/WOCS 14020



(b) Two signals at $P_{rot} = 4.4$ and 4.5 days, suggestive of differential rotation.

Campaign 5 EPIC 211421624/WOCS 12020

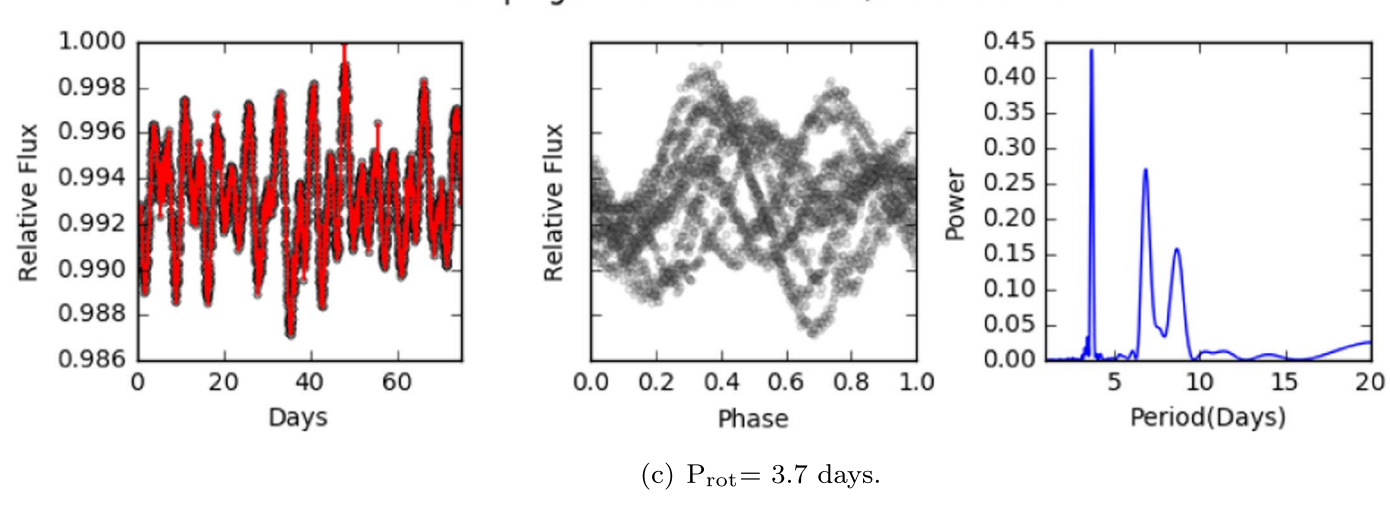
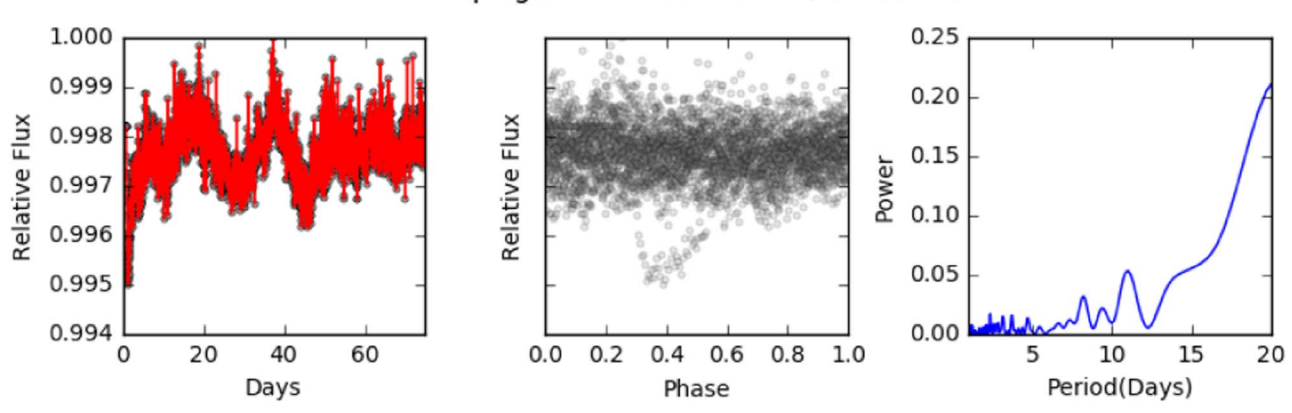
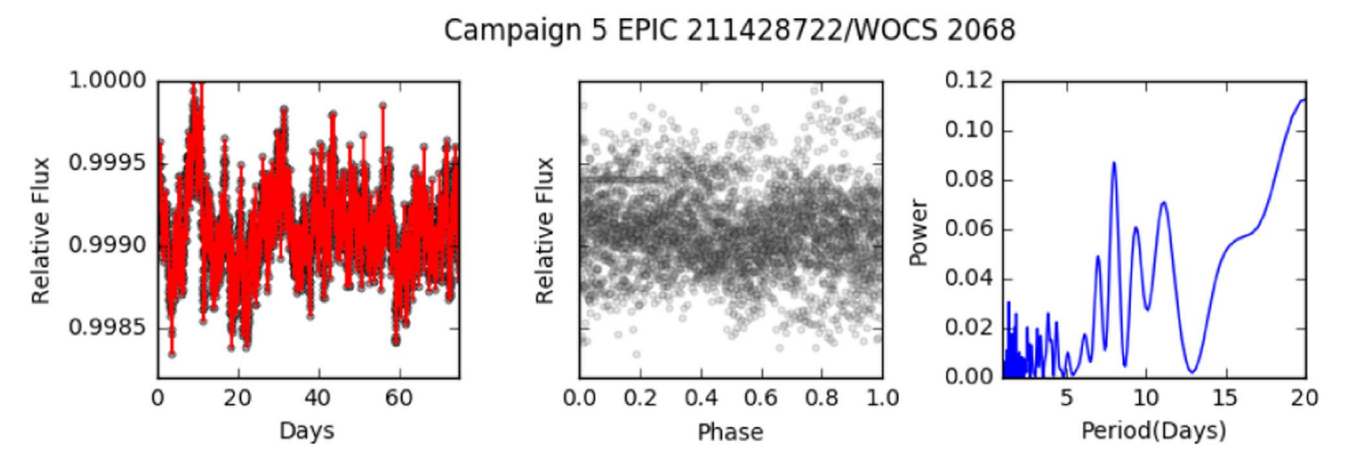


Figure 3. Light curves and periodograms of 11 MS rapid rotators from K2 Campaign 5 (red and blue) and Campaign 16 (purple and green). On the left we show the full K2 C5 or C16 light curve for each star. In the middle we show the phased light curve folded on the dominant period, with the y-axis scaled as in the left panel. On the right we show the Lomb–Scargle periodogram for each star.

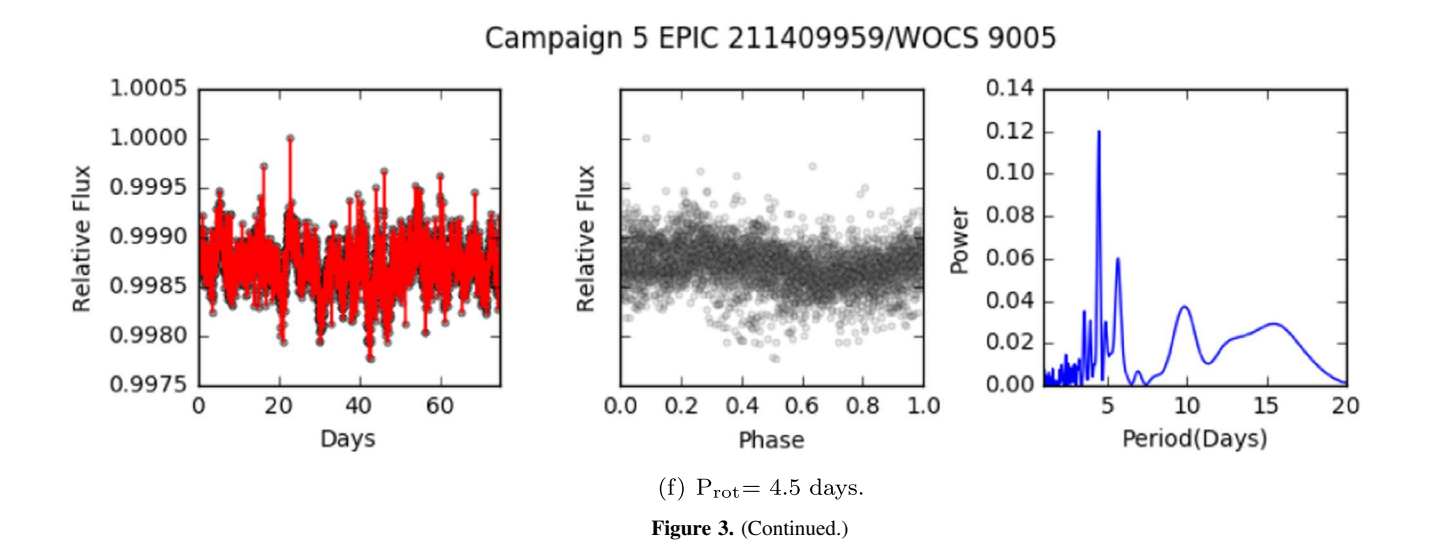
Campaign 5 EPIC 211411928/WOCS 3001



(d) $P_{\text{rot}}=20.5$ days in periodogram; also 3.3 days converted from $v\sin i$. The phased light curve is folded on the 20.5 day period.



(e) Marginal signal at $P_{rot} = 20.3$; phased light curve shows an additional signal at 3.3 days.

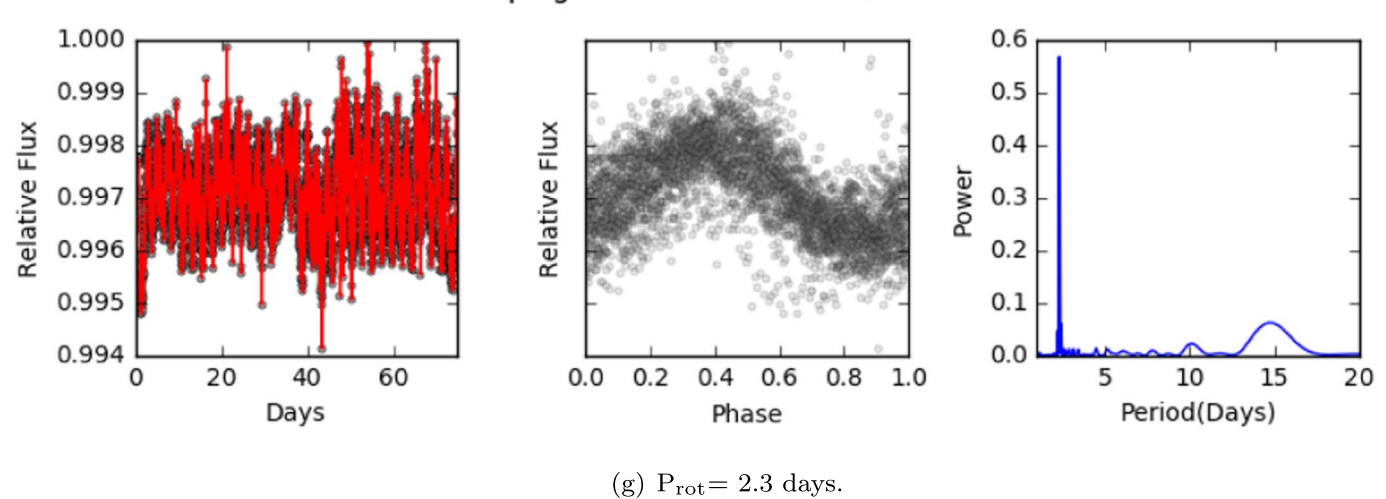


Overall, 2 of 11 stars in our sample are selected based on spectroscopic $v \sin i$ values, and 9 of 11 are selected from K2 light curves. Of these nine stars, five are very secure detections of rapid rotation in which we find the same periods in Campaign 5 light curves from both the Oxford pipeline and

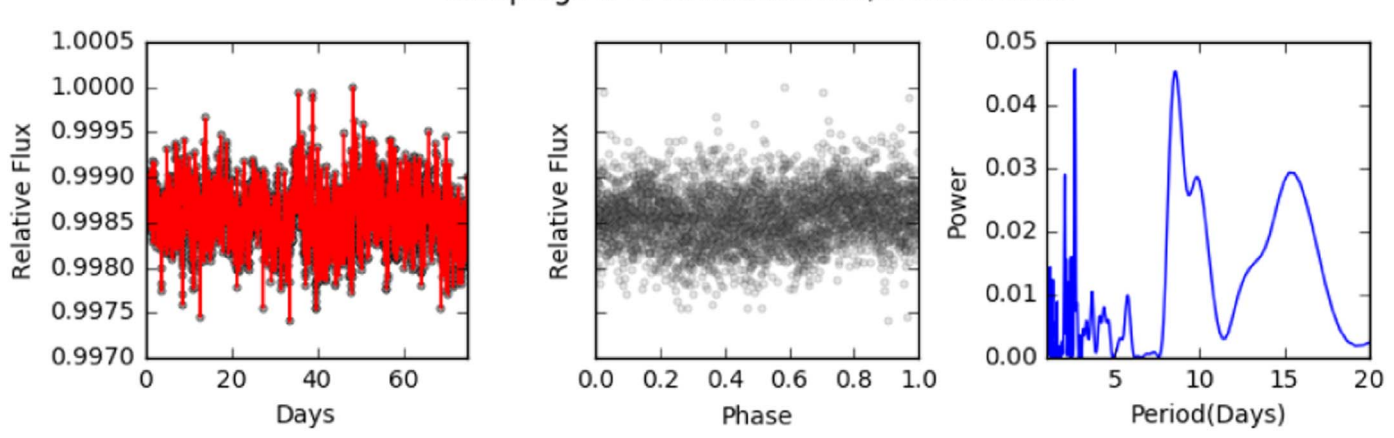
CfA pipeline and detect this period in CfA light curves from Campaign 16.

Four of the nine are less secure detections that have complex signals. These signals are more open to different interpretations or have a higher possibility of being spurious, but we still

Campaign 5 EPIC 211404255/WOCS 6025



Campaign 5 EPIC 211414427/WOCS 11006



(h) Weak signal at $P_{rot} = 2.6$ days, but matches the rotation period converted from $v \sin i$.

Campaign 5 EPIC 211411690/WOCS 2001

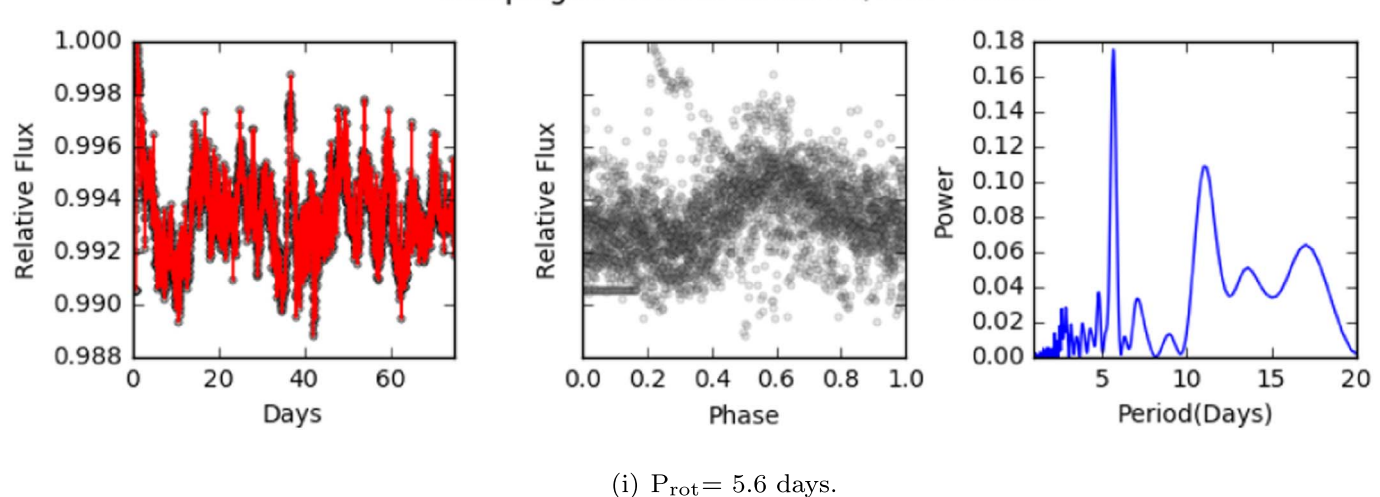
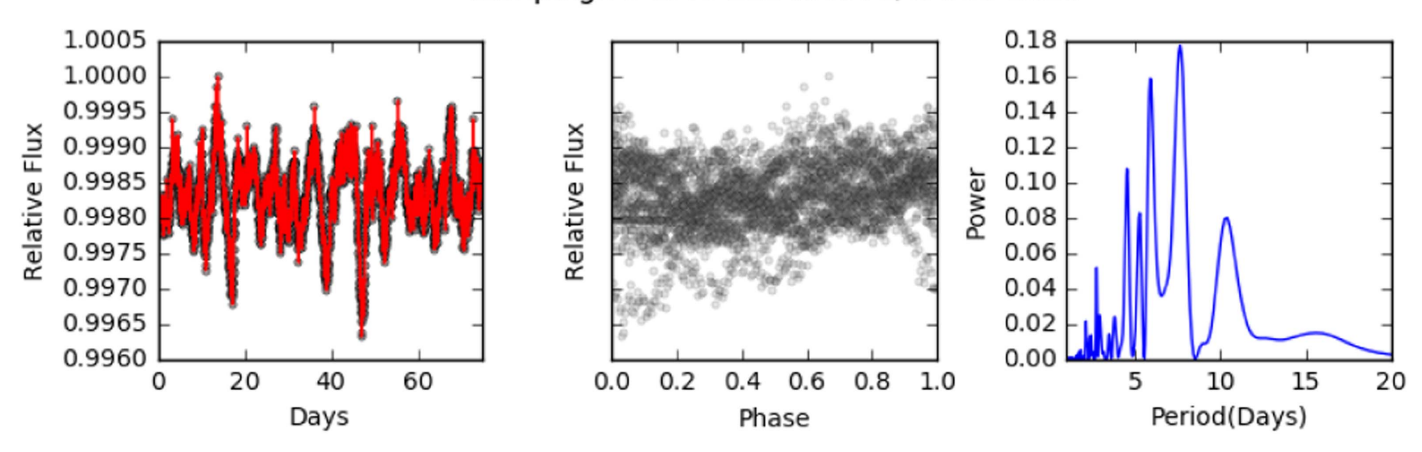


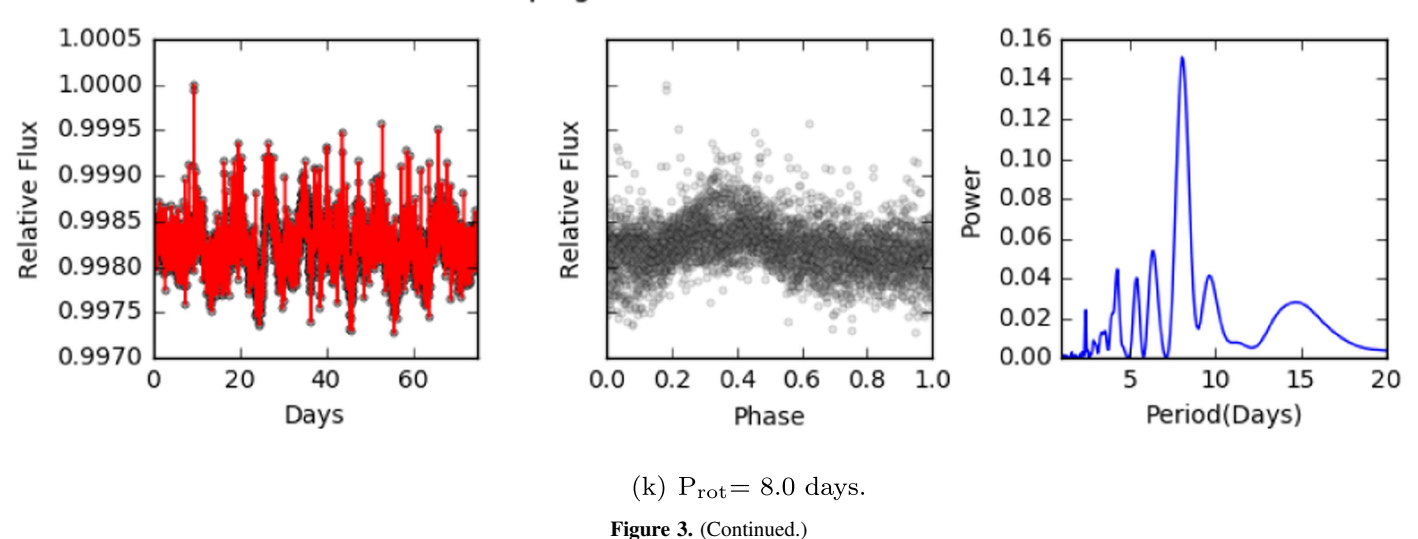
Figure 3. (Continued.)

Campaign 5 EPIC 211406971/WOCS 1020



(j) Multiperiodic with the strongest peak at $P_{rot} = 5.9$ days.

Campaign 5 EPIC 211427425/WOCS 7035



include them as possible detections. We discuss these in detail below.

4.1. Spectroscopic Detections

4.1.1. WOCS 11006

WOCS 11006 is a single-lined spectroscopic binary. We do not have a final orbital solution, so we cannot derive well-constrained orbital parameters. Our radial-velocity observations cover a time baseline of more than 10,000 days and indicate that the binary system is long-period (>3500 days, and perhaps as long as 10,000 days) with a very large orbital eccentricity. The $v \sin i$ derived from the WOCS spectra is $18 \, \mathrm{km \, s^{-1}}$.

The Campaign 5 periodogram for this star shows several low-amplitude peaks, including one at 2.6 days and one at 8 days (Figure 3(h)). A stronger peak at 8 days is measured in a nearby companion, and thus this periodic signal may be background contamination. The 2.6-day peak appears to originate with WOCS 11006. The Esselstein pipeline also measures a periodic signal of 2.6 days, though it is below their

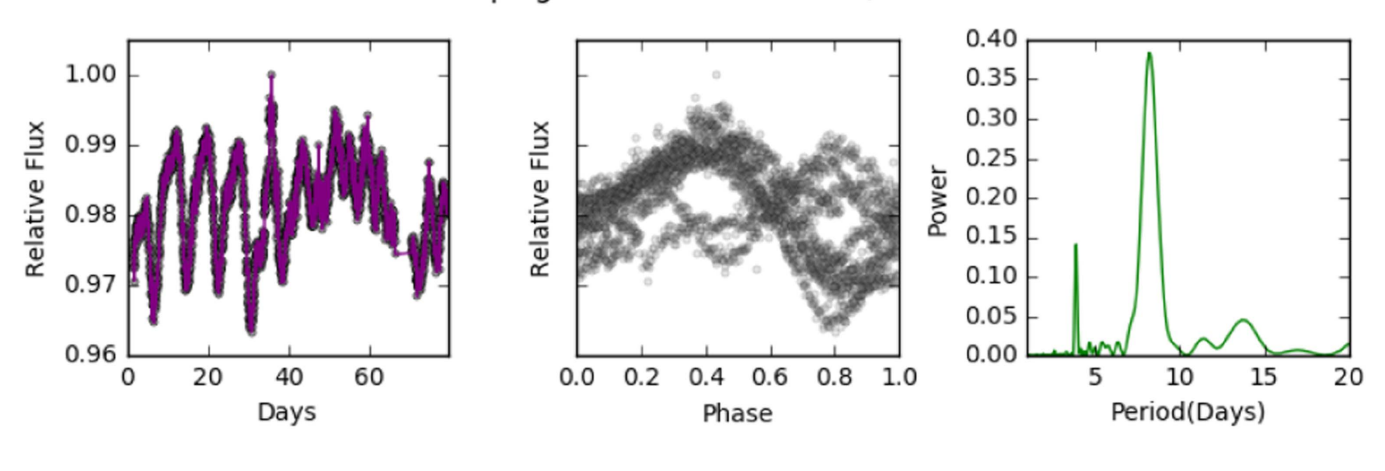
secure-detection threshold. The C16 light curve also shows a weak signal at a similar period of 3 days (Figure 3(s)). These signals are all low confidence, and we would not include this star in our sample based on the periodogram alone. However, the $v \sin i$ conversion suggests a rotation rate of $2.6^{3.4}_{1.4}$ days, providing additional evidence that the photometric rotation period is real. We adopt this 2.6-day rotation period for our analysis.

4.1.2. WOCS 3001

WOCS 3001 is a circular, 128-day single-lined spectroscopic binary that is the bluest star in our sample and notably bluer than the rest of the MS (Figure 2). Despite its color, it has not usually been identified as a BSS in the literature because it is fainter than the MS turnoff, and it was not included in the Geller et al. (2015) sample of BSSs. The detection of this star's elevated rotation rate provides additional evidence that it is indeed a relative of the BSSs.

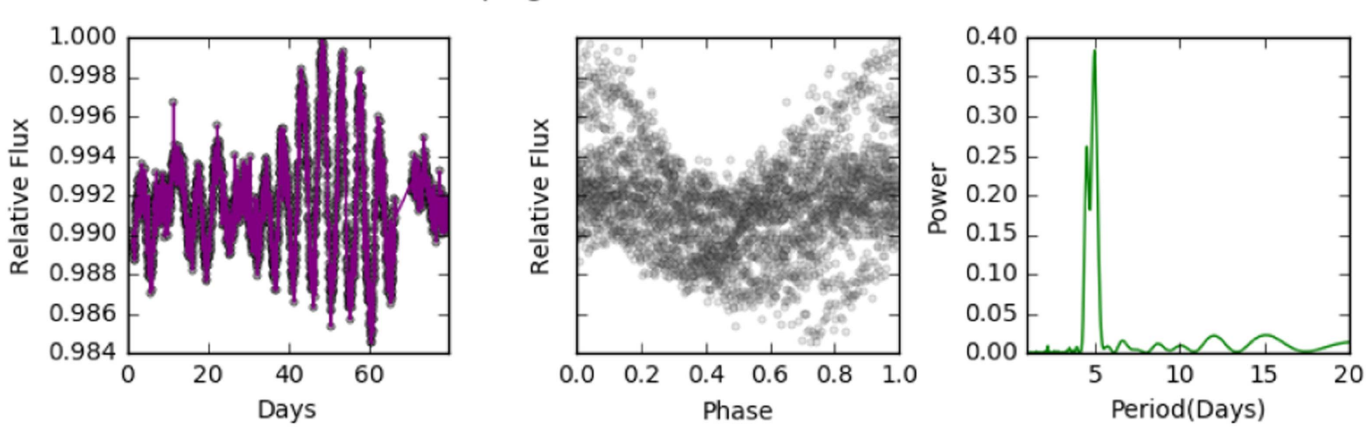
The $v \sin i = 14.7 \text{ km s}^{-1}$ measurement indicates that WOCS 3001 is a rapid rotator. However, WOCS 3001 does not show a

Campaign 16 EPIC 211411716/WOCS 4001



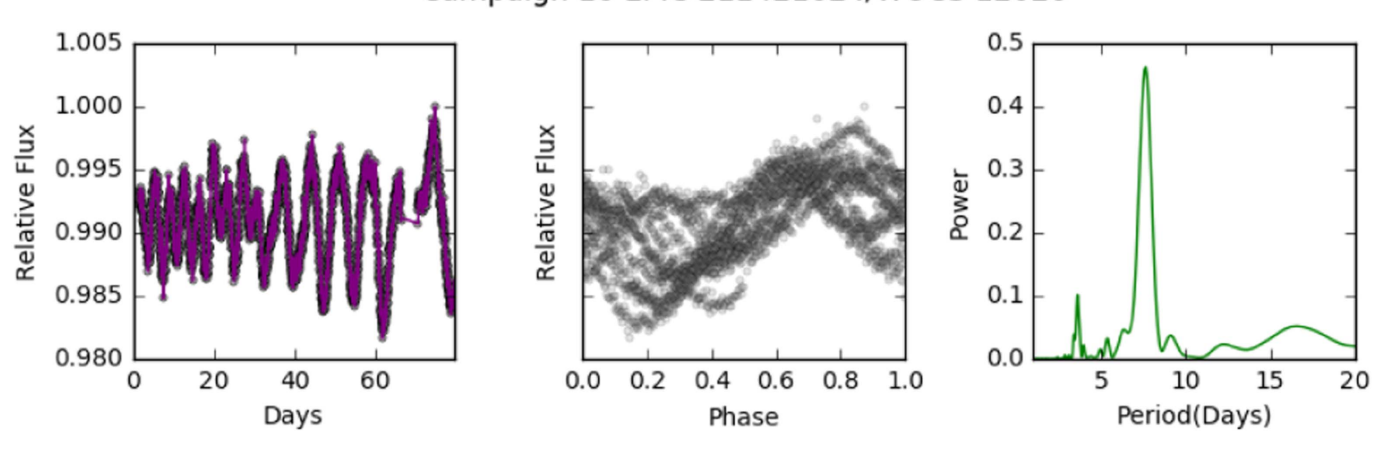
(l) $P_{rot} = 7.9$ days as in C5.

Campaign 16 EPIC 211410278/WOCS 14020



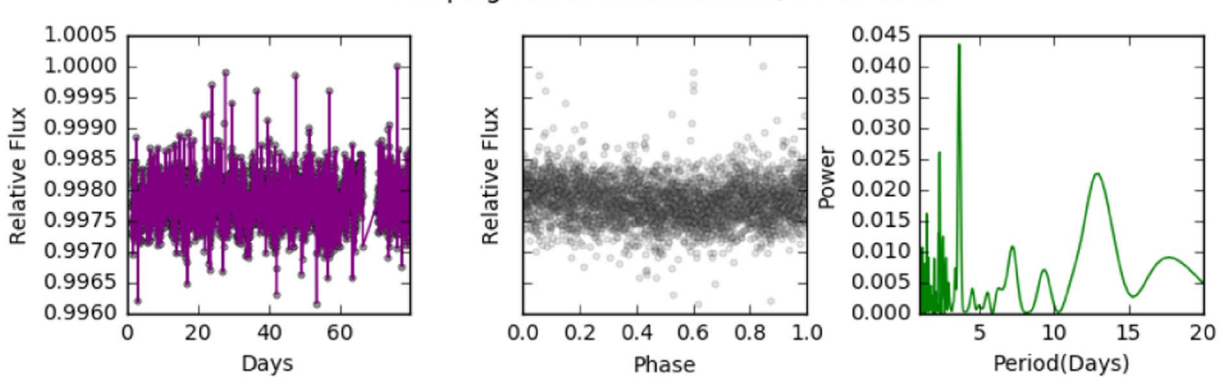
(m) Two signals at $P_{\rm rot}$ = 4.4 and 4.5 days, suggestive of differential rotation as in C5.

Campaign 16 EPIC 211421624/WOCS 12020

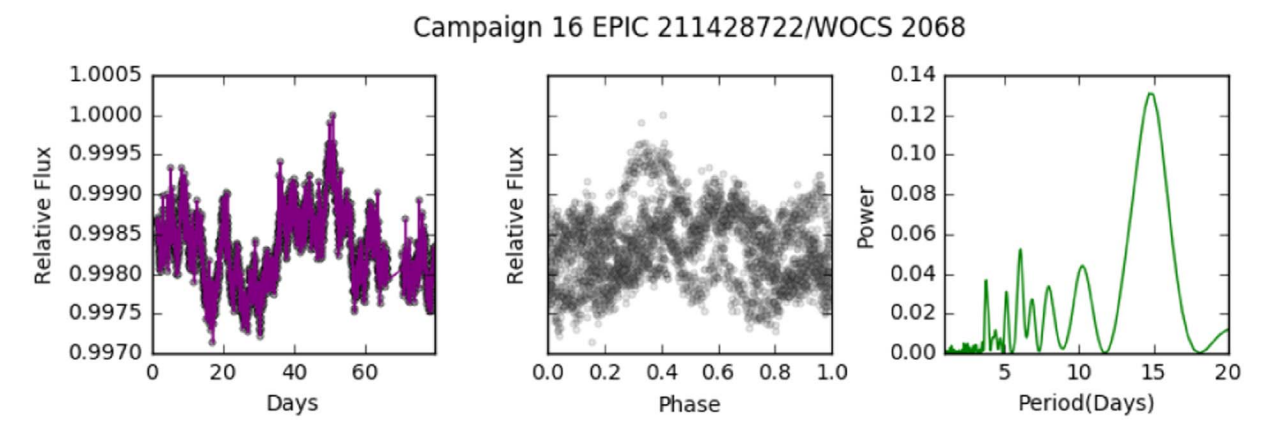


(n) P_{rot} = 7.6 days, twice the period of C5 Figure 3. (Continued.)

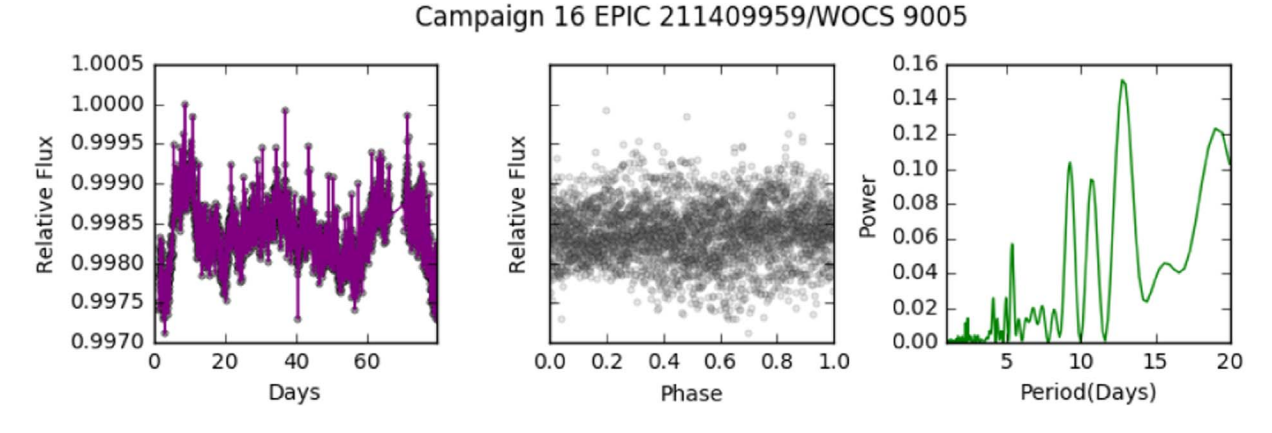
Campaign 16 EPIC 211411928/WOCS 3001



(o) $P_{\text{rot}}=3.3$ days converted from $v\sin i$. The C16 light curve shows a very weak peak at P=3.6, consistent with the spectroscopically derived rotation, which we use to fold the light curve.



(p) In C16 light curve shows variability at short periods as well as a marginal signal at longer periods (P= 15 day), similar to C5.



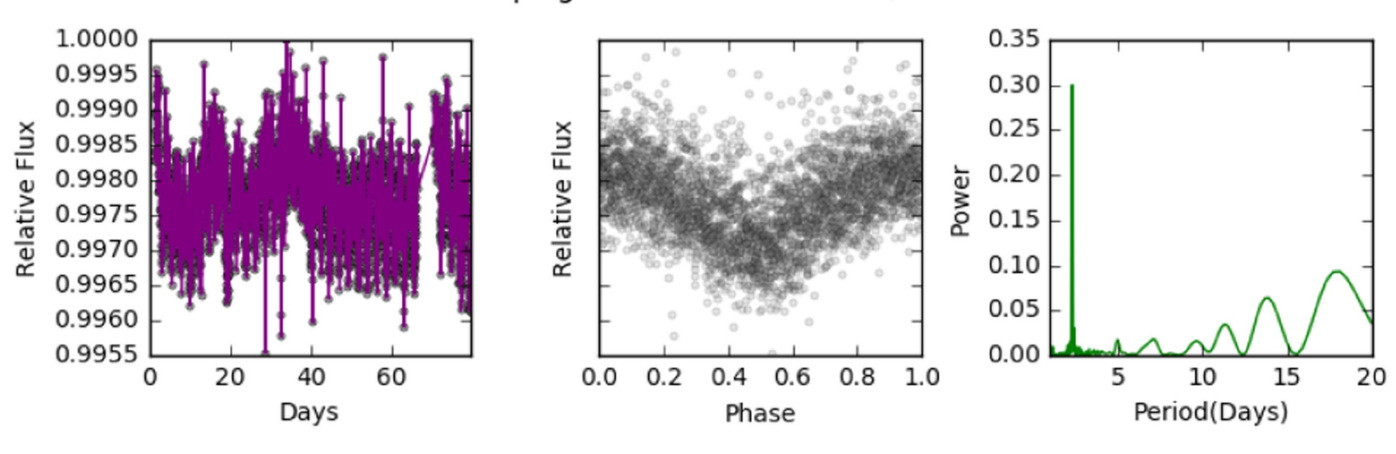
(q) P_{rot} = 4.5 days in C5. A much lower-amplitude signal around 5 days can be seen in the C16 power spectrum, but it is not clearly significant. Light curve is phased on the C5 period.

Figure 3. (Continued.)

rotation signal at short periods in the Campaign 5 periodogram (Figure 3(d)), and in C16 it shows only a very weak signal (P = 3.6 days) that is not significant (Figure 3(o)), though it is consistent with rotation period inferred from the $v \sin i$ measurement. The C5 light curve does suggest a 20-day rotation signal,

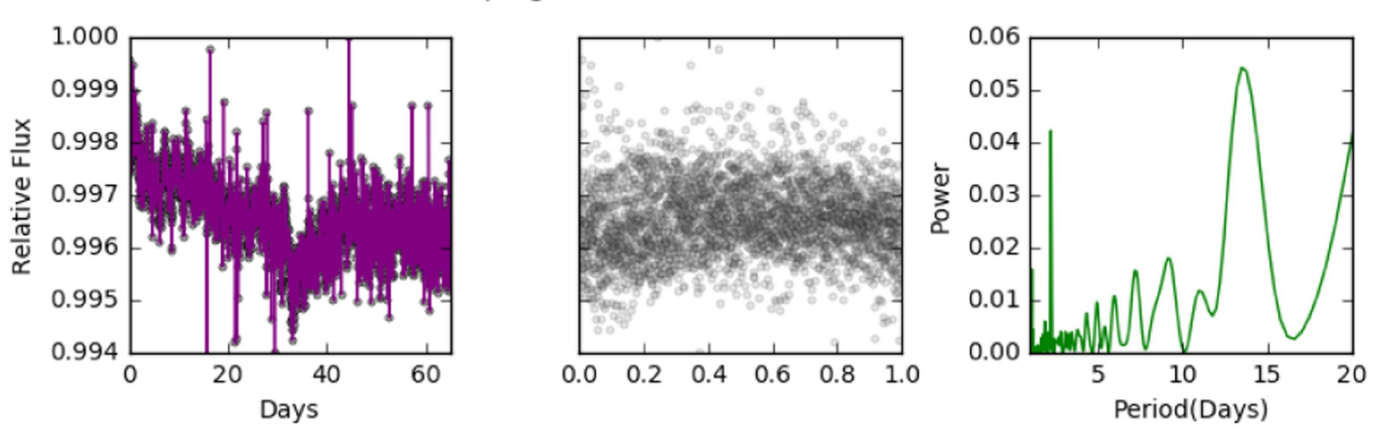
although due to the 75-day time baseline of the *K*2 observations, the detection of such long-period variability is not secure (Esselstein et al. 2018). Due to its unusually hot temperature for the cluster, WOCS 3001 is near the divide between stars with convective envelopes and those with radiative envelopes. As a

Campaign 16 EPIC 211404255/WOCS 6025



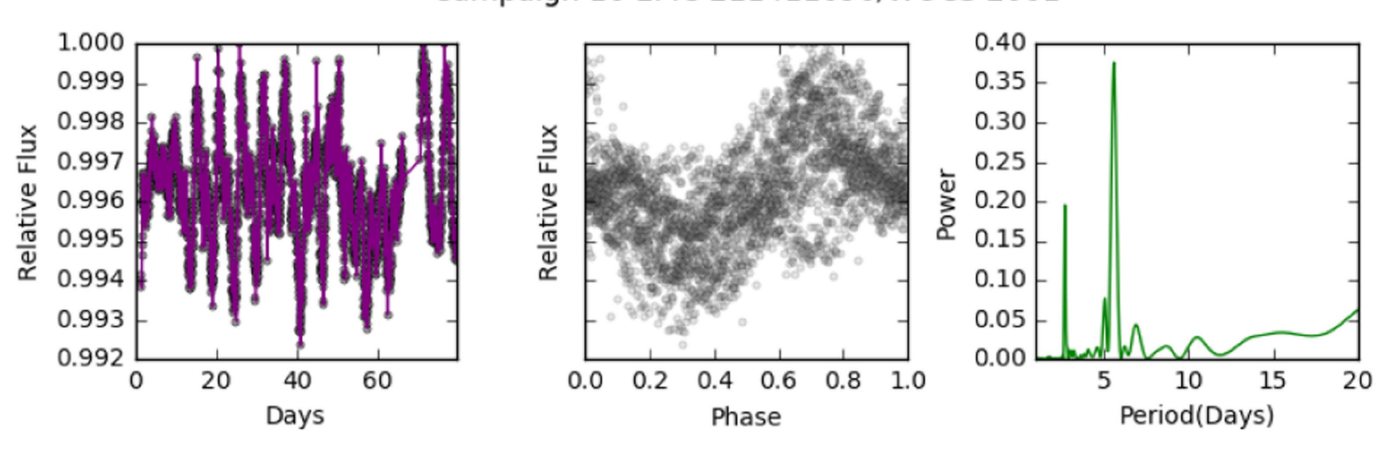
(r) $P_{rot} = 2.3 \text{ days}$, as in C5.

Campaign 16 EPIC 211414427/WOCS 11006



(s) Low signal P = 2.2 days in C16, similar to C5.

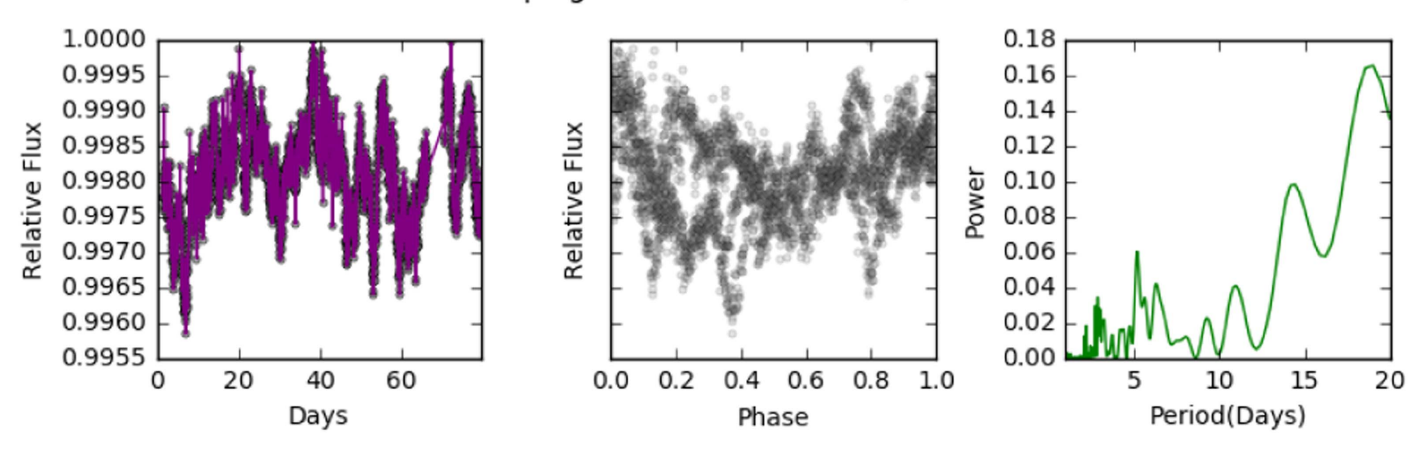
Campaign 16 EPIC 211411690/WOCS 2001



(t) P = 5.6 days as in C16, same as C5.

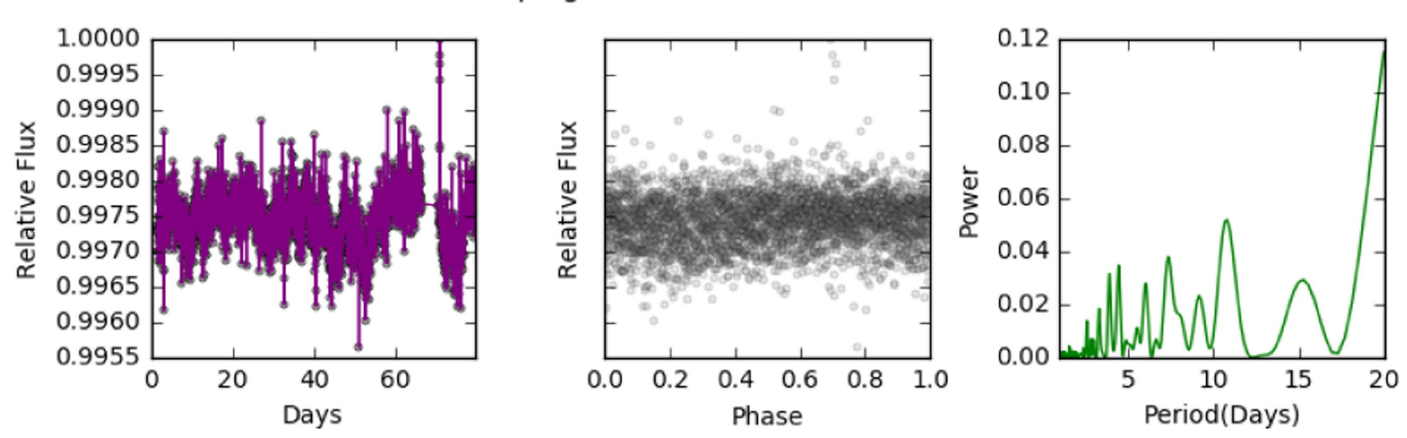
Figure 3. (Continued.)

Campaign 16 EPIC 211406971/WOCS 1020



(u) C16 light curve shows lower amplitude peaks near 5 days

Campaign 16 EPIC 211427425/WOCS 7035



(v) No Significant peaks in C16. $P_{\rm rot}=8.0$ days in C5. Lightcurve is phased on the 8.0 day signal from C5. Figure 3. (Continued.)

result, it is possible that the star could be a rapid rotator without significant evidence of spot modulation.

The Esselstein approach measures a signal at 2.3 days in the C5 light curves that is below their secure-detection threshold and does not detect the 20-day signal.

Given the low reliability of all the measured signals, we conclude that there is no clear period evident in the K2 light curves. In the analysis that follows, we adopt a rotation period of 3.3 days, which we derive from the $v \sin i$ measurement using the technique outlined in Section 2.

4.2. Secure Photometric Detections

We find five stars with strong peaks in their periodograms. The shape of the light curves, clear periodicity, and evolving light-curve amplitude are characteristic of variability caused by starspots. We therefore consider these clear detections of spot modulation, and that the periodic signals can be used to measure the stellar rotation periods.

4.2.1. WOCS 14020

In Campaign 5, WOCS 14020 shows two strong peaks in its periodogram, one at 4.4 days and one at 4.5 days (Figure 3(b)). The Campaign 16 light curves show the same signals (Figure 3(m)).

A rotation period of 4.4 days is also detected using the Esselstein et al. (2018) pipeline. The light curve (Figures 3(b), (m)) also shows a clear beating pattern. Given the close spacing of these two peaks, we suggest that the two periods are evidence for differential rotation on the star, with two starspots at slightly different latitudes moving in and out of phase with each other (e.g., Reinhold & Gizon 2015).

The spectrum of this star is single lined, and the mass function sets a minimum companion mass of $0.15\,M_\odot$. The lack of flux from a companion in the spectrum combined with the very low minimum mass strongly suggests either a WD or an M-dwarf secondary star. Interestingly, the system is detected in both the *Galaxy Evolution Explorer* (*GALEX*) near-UV and far-UV (FUV) filters (effective wavelengths of $\lambda_{\rm eff} = 2267$ and 1516, respectively; Martin et al. 2005), indicating that the

Table 1
Stellar and Orbital Properties of Rapid Rotators

EPIC ID	WOCS ID	Orbital Period ^a (days)	Eccentricity ^a	$f(m)^{\mathbf{a}}$ (M_{\odot})	V^{b}	$B-V^{b}$	Rotation Period (days)	Membership ^c
211411716	4001	139.77	0.36	2.17e-2	15.21	0.79	7.9	BM
211410278	14020	358.9	0.23	$2.38e{-3}$	14.58	0.67	4.4	BM
211421624	12020	762	0.056	2.87e - 2	14.28	0.59	7.6	BM
211411928	3001	128.14	0.04	$1.43e{-2}$	13.26	0.46	3.3 ^d	BM
211428722	2068	8567	0.859	$6.81e{-2}$	12.19	0.55	20 and 3	BM
211409959	9005	2769	0.15	$3.68e{-2}$	12.65	0.52	4.5	BM
211404255	6025	6265	0.38	2.20e - 1	13.70	0.6	2.3	BM
211414427	11006	>3500			13.33	0.50	2.6 ^d	BLM
211406971	1020				12.70	0.48	5.9	SM
211411690	2001				13.24	0.60	5.6	SM
211427425	7035				13.36	0.57	8.0	SM

Notes.

system has a large UV excess. We show the spectral energy distribution (SED) in Figure 7(b). The *GALEX* FUV measurement supports the presence of a hot, faint companion, likely a WD star. The FUV flux excess is consistent with a $\sim\!13,\!000$ K C/O WD. This temperature implies an age of $\sim\!300\,\mathrm{Myr}$ (Tremblay et al. 2011), in general agreement with the age implied from the rotation rate of $\sim\!200\,\mathrm{Myr}$.

Narrowband UV photometry and/or UV spectroscopy are needed to confirm this detection and provide better temperature and age estimates.

4.2.2. WOCS 4001, 6025, 12020

These systems are all single-lined spectroscopic binaries. WOCS 6025, 4001, and 12020 have very clear signatures of spot modulation in their C5 and C16 light curves at levels of up to a few percent, as well as strong peaks in their CfA periodograms with periods consistent between C5 and C16 and that are independently confirmed by Esselstein.

WOCS 4001 has a clear period of P = 7.9 days in both C5 and C16 light curves (Figures 3(a), (1)). The Esselstein pipeline produces a slightly longer period of P = 8.0 days. It is located in the cluster core and thus has many bright neighbors that we examine carefully to determine whether they may be contaminating the light curve. A bright (Kp = 12.69) nearby star (WOCS 1001) does display variability at a similar period, but a comparison of the light curves reveals that they have different shapes and are out of phase with each other.

For WOCS 12020, the Campaign 5 light curve shows the strongest peak at P=3.7 days, with a lower peak at twice this period (Figure 3(c)). In contrast, Campaign 16 shows that the strongest peak is P=7.6, with the 3.7-day period the secondary peak (Figure 3(n)). It can happen that a star has two spots on opposite sides, causing significant periodicity at half the true rotation period. We therefore interpret 7.6 days as the true period, which we report in Table 1.

WOCS 6025 has a period of P = 2.3 in C5 and C16 light curves (Figures 3(g), (r)) and is also detected in the Esselstein light curves with the same period.

All three stars are long-period ($P_{\rm orb} > 100$ days) binaries. All but WOCS 6025 have secondary-mass limits consistent

with WD companions and thus with being candidate post-mass-transfer systems (Figure 6). WOCS 6025 has a large secondary-mass limit of $1.1\,M_\odot$, more compatible with an F- or G-type MS star, though the spectra and the SED of the system do not reveal any evidence of such a companion. Another possibility could be that the system is a triple system composed of a near-turnoff primary star and a secondary that is a close binary composed of two low-mass stars ($\sim 0.5\,M_\odot$). If these stars were tidally locked in a 2.3-day orbit, this could also explain the origin of the periodic signal.

4.2.3. WOCS 2001

WOCS 2001 shows a strong single peak at P=5.6 days in both the C5 and C16 periodograms (Figures 3(i), (t)). This period is also confirmed by the Oxford pipeline measurements. WOCS spectra indicate that the star is not a velocity variable, and therefore we classify it as single. If this star has a binary companion that is not spectroscopically detected, it must be wide ($P_{\rm orb} \gtrsim 10,000$ days) or viewed very close to face-on. (Although if the rotation and orbital axes are aligned, being face-on would make detecting a photometric rotation period unlikely.)

Assuming that it is a true single star, this system would not have formed from mass transfer or a Kozai-induced merger in a triple system, as both scenarios are expected to leave behind binary systems. A merger of a close MS binary system through internal processes such as magnetic braking (e.g., Andronov et al. 2006) or a dynamical scenario may also be a plausible origin. Dynamical collisions often leave the collision product bound in a binary or higher-order system. The collision product may also be left as an unbound single star like WOCS 2001, although this outcome is less probable (Fregeau et al. 2004).

4.3. Possible Photometric Detections

4.3.1. WOCS 2068

WOCS 2068 is a long-period (8567 days), highly eccentric (e = 0.859) binary. The SED of the system suggests that the binary consists of two stars near the MS turnoff (see Figure 7(e) and Section 5.4). One of these stars has an unusually hot

^a From A. M. Geller et al. (2019, in preparation).

^b From Geller et al. (2015) original photometry from Montgomery et al. (1993).

^c Membership classifications are explained in Geller et al. (2015). BM = Binary member; BLM = Binary Likely Member; SM = Single Member.

^d These stars are included based on their $v \sin i$ measurements ($v \sin i > 10 \text{ km s}^{-1}$), not periodic signals in their K2 light curves.

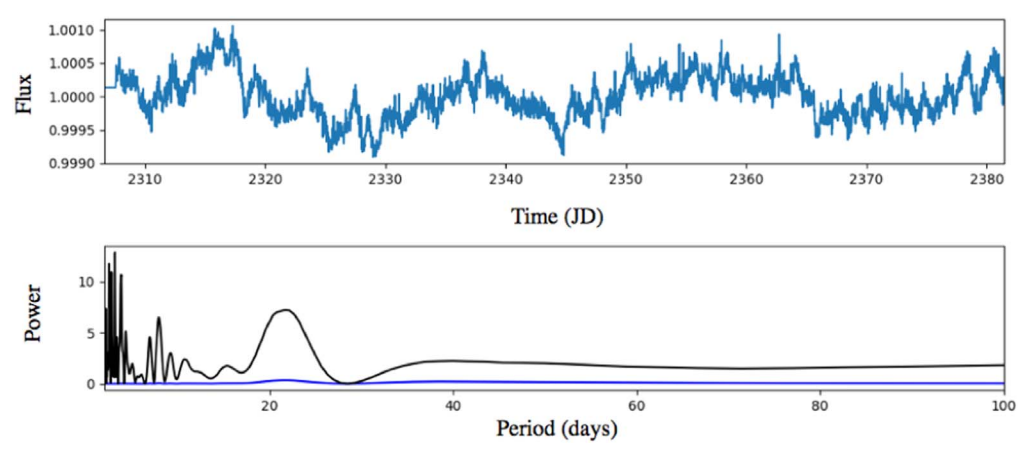


Figure 4. Light curve (top) and power spectrum (bottom) of WOCS 2068 from the pipeline of Esselstein et al. (2018). In the power spectrum, the blue line shows the raw power and the black line shows the normalized power as defined in Esselstein et al. (2018). The normalized power spectrum shows the strongest power at \sim 3 days, as well as a signal at 20 days, though the multiperiodic nature of the star and relatively low amplitude put it below their formal detection criteria.

temperature for the cluster, placing it slightly to the blue of the MS turnoff and suggesting that it is a BSS. The other is located on the cluster turnoff.

This star is multiperiodic, showing a marginal period detection of 15–20 days, as well as multiple peaks at shorter periods indicating variability on a timescale of several days.

In Figure 3, we have folded the C5 and C16 light curve on the dominant period of either 15 or 20 days (Figures 3(e), (p)). The phase-folded light curve shows additional variability on shorter-period timescales (\sim 3 days). The Oxford pipeline also yields a \sim 3- and 20-day rotation period, though the multiperiodic nature of the star and the relatively low amplitude put it below the detection criteria from Esselstein et al. (2018). We show the light curve and power spectrum from the Oxford pipeline in Figure 4.

We note that although the 15- to 20-day period technically shows more power in Figures 3(e) and (p), longer-period signals are much more likely to be spurious owing to the *K*2 instrumental systematics. Detections of short-period variability, even at lower power, are more reliable (see Esselstein et al. 2018 for a detailed discussion).

We consider this a strong detection of short-period variability, but due to the complexity of the light curve and the low amplitude of the variability, we cannot measure a precise period or definitively attribute the variation to rotation. The short-period signals in the light curve may be consistent with small spots on a rotating star, but they could also be consistent with stellar pulsation. Normal turnoff stars in M67 are not in the instability strip, nor are they observed to be pulsating. However, the unusually hot 6800 K companion inferred from the SED fit (Section 5.4) would be near the red edge of the γ Doradus region (Handler 1999; Balona 2018), and it can be difficult to differentiate between rotation and γ Doradus pulsations (Balona et al. 2011; Rebull et al. 2016). However, γ Doradus pulsators usually have periods of 0.4–3.0 days (Kaye et al. 1999), somewhat shorter than the timescale of the variability of this source.

Regardless of the interpretation of the light curve, it is likely that the system has been through a stellar interaction of some kind given that the SED indicates that one component is hotter than the cluster MS turnoff and is either a rapid rotator or a pulsator, neither of which would be expected for a normal MS star in the cluster.

If we attribute the observed periodicity to be rotation, it suggests that the system is composed of one slowly rotating MS star with a period of 15–20 days, typical for the cluster, though we stress that this longer period may be due to K2 systematics rather than true stellar variability. The other star in the system has a short rotation period of \sim 3 days. The system is not an MS-WD binary, the expected outcome of mass transfer formation. It is unlikely that a WD would have been ejected from this system in a dynamical encounter given the expected encounter rates in M67 and the young age of the system inferred from its rapid rotation (Leigh & Sills 2011). Mass transfer is therefore not a likely explanation for this system. Instead, it may be a merger or dynamical collision. In such a merger scenario, the initial system may have been a hierarchical triple consisting of a short-period inner binary and a distant triple companion. The inner binary was then driven to a merger, either by magnetic braking or through Kozai-Lidov oscillations, with the former tertiary now the observed wide secondary.

Alternatively, the system may have resulted from a dynamical encounter involving at least one binary star in which two stars collided (e.g., Leonard 1989; Sills et al. 2001). Scattering experiments show that binary systems resulting from dynamical collisions tend to result in very high eccentricity orbits (Fregeau et al. 2004), as is seen in this system. In contrast, a merger of an inner binary in a triple system does not favor any particular eccentricity (Naoz & Fabrycky 2014), and mass transfer origin preferences low-eccentricity outcomes (e.g., Figure 5).

Additionally, this binary is located in the cluster halo, not in the core as is expected for most binaries because of mass segregation. Dynamical encounters can impart a recoil velocity to a star (e.g., Phinney & Sigurdsson 1991), pushing the orbit farther into the halo or perhaps ejecting it entirely, which could explain this binary's less probable location within the cluster.

Taking this information together, the properties of WOCS 2068 may fit best with a recent stellar dynamical encounter that resulted in the collision of two MS stars. A merger in a triple system is also possible, but a mass transfer origin is not consistent with the observed system.

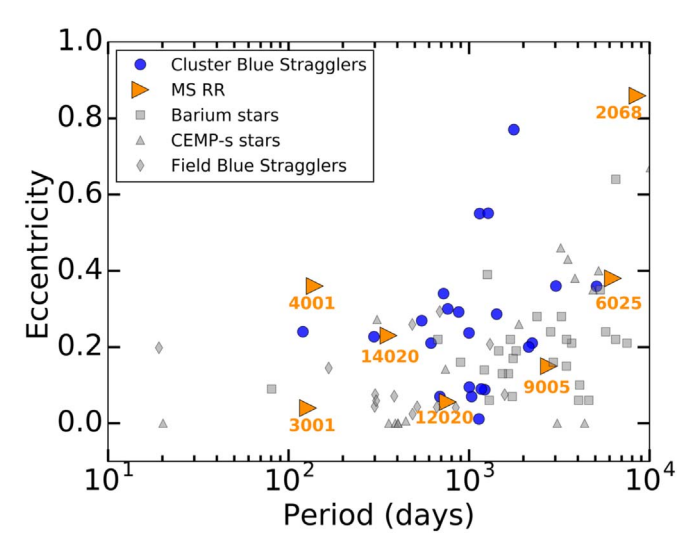


Figure 5. Comparison of the distributions of periods and eccentricities of the M67 MS rapid rotators (orange triangles) to the binary BSS populations of several old open clusters (blue circles) and post-mass-transfer binaries observed in the field (gray symbols), including CEMP-s stars (Hansen et al. 2016), field BSSs (Carney et al. 2005), and barium stars (Jorissen et al. 1998). We do not include the rapid rotator WOCS 11006 in this diagram, as we do not have a complete orbital solution, but it appears to be a long-period, high-eccentricity system that would fall in the upper right corner of this diagram.

4.3.2. WOCS 9005

WOCS 9005 is a long-period binary system showing periodicity in the C5 light curve at P=4.5 days (Figure 3(f)). The same period is detected using the pipeline of Esselstein et al. (2018), but the amplitude is below their secure-detection threshold. Our visual inspection confirms a single, clean periodic signal in the periodogram and visible variability in both phased and unphased light curves matching this period. However, the C16 light curves do not show strong periodicity at this or any other period (Figure 3(q)). There is a slight peak near 5 days, and visual examination of the light curve suggests that a low-amplitude \sim 5-day signal may be visible at the beginning of the C16 campaign, which disappears over the course of the observations. These features may hint at the presence of a rotation signal in C16, but they are not conclusive.

It is possible that a small spot(s) on the star during C5 was (were) weaker or no longer present during the C16. It is also possible that the signal visible in C5 was spurious. Given the strong detection in C5, we include 9005 in our sample but caution that the detected period needs confirmation.

4.3.3. WOCS 7035 and 1020

Both WOCS 7035 and WOCS 1020 are non-velocity-variable. If these stars do have companions that have avoided detection, these systems are either wide ($P_{\rm orb} \gtrsim 10{,}000$ days) or viewed close to face-on.

The C5 light curve of WOCS 7035 shows a single peak in its periodogram at 8.0 days, in agreement with the ACF period of Esselstein (Figure 3(k)). However, we observe no strong periodicity in the C16 light curve (Figure 3(v)). As with 9005, we include WOCS 7035 in our sample with caution.

WOCS 1020 shows several closely spaced peaks in the C5 periodogram, with the strongest at 5.9 days (Figure 3(j)). Esselstein does detect variability in this star with a similar period in the Oxford and CfA light curves but does not classify it as a significant detection owing to the multiperiodic nature.

The C16 light curve again shows multiperiodic variability, but with a lower-amplitude signal around 5 days (Figure 3(u)). It also shows a longer-period signal around 20 days, but such long-period signals are not very reliable in K2 data. Esselstein et al. (2018) introduce a process to normalize periodograms to remove background signals at long periods, which we have not done here, and given the lack of detection of a long-period signal in C5 in both pipelines, it is not clear whether this signal is significant.

While this star is clearly variable, the nature of the variability is not certain. The light curve could be consistent with multiple small starspots, but as with WOCS 2068, this star has an SED temperature that places it in the γ Doradus region (Section 5.4). However, the 5.9-day period is more consistent with a rotation signal than the typical 0.4- to 3.0-day periods of γ Doradus variables (Kaye et al. 1999). We therefore classify this star as a probable rapid rotator.

If these stars are both rapidly rotating single stars, they would not have formed from mass transfer or Kozai-induced mergers in triple systems, as both scenarios are expected to leave behind binary systems. Instead, they may have formed through dynamical collisions between MS stars as we suggest for WOCS 2001.

Another possibility is a merger of a close MS binary system through internal processes such as magnetic braking (e.g., Andronov et al. 2006).

5. Characteristics of Rapid Rotators

In Figure 2 we mark the location of these 11 stars in a CMD of M67 members. For reference, in Figure 1 we show the rotation periods of these stars compared to normally rotating stars in M67 (Barnes et al. 2016) and rotation periods predicted by the gyrochronology relations of Angus et al. (2015). We discuss the properties of this sample below.

5.1. Binary Fraction

Eight of the 11 systems in our sample are binaries, for a binary fraction of $73\% \pm 31\%$.

For comparison, the spectroscopic binary fractions ($P_{\rm orb}$ < 10^4 days) of M67 and other old open clusters are observed to be in the range of 20%–30% (Geller et al. 2009; Milliman et al. 2014; Geller et al. 2015). These rapid rotators thus have about 3 times the binary fraction expected for a typical MS population.

Classical BSS populations in old open clusters are observed to have similarly high binary fractions. In M67 itself, the BSS binary fraction is 80% (Geller et al. 2015). In the 7 Gyr open cluster NGC 188, $76\% \pm 19\%$ of BSSs are observed to be spectroscopic binaries within a similar period domain (Mathieu & Geller 2009). Thus, the observed high binary fraction among these rapid rotators is consistent with our hypothesis that they are lower-luminosity analogs of the BSSs formed through similar binary evolution channels.

5.2. Orbital Properties

We show the eccentricity–period distribution of the eight binaries in our sample in Figure 5. For comparison, we also show the eccentricity–period distribution of field barium stars, CEMP-*s* stars, blue metal-poor stars, and BSSs in the old open clusters NGC 188 (Geller et al. 2009), M67 (A. M. Geller et al. 2019, in preparation), and NGC 6819 (2.5 Gyr; Milliman et al. 2014).

Most of the binaries in our sample of rapid rotators have low eccentricities that fall within the eccentricity—period locus of these other post-mass-transfer binaries.

Typical populations of long-period solar-like MS binaries have eccentricities in a Gaussian-like distribution about a mean of e=0.4 (e.g., Meibom et al. 2006; Raghavan et al. 2010). On the other hand, post-mass-transfer binaries show lower eccentricities, presumably because these systems go through substantial tidal dissipation before the onset of Roche lobe overflow. Even though BSSs and the other post-mass-transfer binaries often do not have circularized orbits, they do show lower eccentricities than solar-type MS binaries at orbital periods of ~ 1000 days (Jorissen et al. 1998, 2016; Carney et al. 2005; Mathieu & Geller 2009; Hansen et al. 2016). Some do have circular orbits, as do two binaries in our sample of rapid rotators (WOCS 3001 and WOCS 12020), suggestive that both of these systems have been through mass transfer.

Two of the eight binaries, WOCS 11006 and 2068, have much larger eccentricities and longer periods than typical. Such large eccentricities are perhaps more compatible with dynamical formation, as we suggest for WOCS 2068 (Section 4.3.1).

We note that three of the binaries in our sample (WOCS 3001, 4001, 14020) have orbital periods of just a few hundred days, shorter than all but three of the observed BSSs in NGC 188, M67, and NGC 6819. If these stars are indeed post-masstransfer binaries, their orbital periods suggest that they result from case B mass transfer (mass transfer from a red giant branch donor). These three short-period systems resemble WOCS 5379 in the cluster NGC 188, a 120-day BSS-WD binary. Gosnell et al. (2019) measure a precise WD mass for WOCS 5379 and demonstrate that it is a helium WD and thus formed from case B mass transfer. However, this observation is difficult to resolve with mass transfer theory because a wide range of models and assumptions predict that case B mass transfer in this systems should have resulted in a common envelope and a likely merger. Like WOCS 5379, these three short-period systems in M67 may be interesting probes of mass transfer theory and the criteria for common-envelope evolution.

Additionally, it is interesting that more of these short-period systems show up in this lower-luminosity domain than among the BSS population. This could hint that they form from binary systems with initially lower-mass secondaries that are not expected to evolve through stable mass transfer, or that they do not accrete as much mass from their companions and are indicative of more inefficient mass transfer than the BSSs. These three systems are excellent candidates to model in more detail, as their evolutionary pathways may help constrain these uncertain aspects of mass transfer physics.

5.3. Companion Masses

For seven of the eight binaries in our sample, we have orbit solutions that enable us to determine a binary mass function, f(m). From this function, we can derive lower limits on the mass of the secondary after adopting a mass for the primary. We do this by fitting a stellar evolutionary track to the CMD position of each system, recognizing that standard stellar evolution theory may not be accurate for these stars. We find that the primary stars range in mass from 0.9 to $1.35\,M_{\odot}$. Using these primary masses, we derive the minimum mass for each secondary star. These secondary-mass lower limits are shown in Figure 6, plotted against periastron separation.

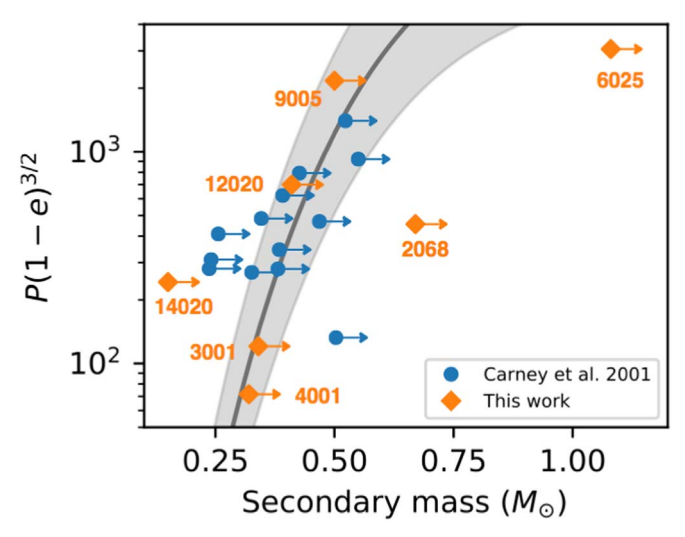


Figure 6. We show orbital separation at periastron and secondary mass for a sample of field BSS binaries from Carney et al. (2001; blue circles) and our sample of rapidly rotating MS binaries (orange diamonds). All points show lower limits on the secondary masses derived from the binary mass functions. We also show in gray the theoretical relationship of Rappaport et al. (1995) between orbital period and WD mass for binaries resulting from stable mass transfer. We note that comparison of the data to the Rappaport relationship is only valid for post-mass-transfer systems with WD companions. WOCS 11006 is not included in the plot, as we have no secure orbital solution.

We find that five of the seven binaries are consistent with the period–secondary-mass range expected for post-mass-transfer MS–WD binaries (Rappaport et al. 1995). Two systems, WOCS 2068 and WOCS 6025, appear to have secondaries more massive than expected if their companions are WDs. This is as expected for WOCS 2068, as the SED indicates contributions from two MS stars (Section 5.4).

WOCS 6025 also has a substantially more massive companion (>1.1 M_{\odot}) than expected for a WD. The WD initial-final mass relation predicts that such a massive WD would form from a very massive progenitor (>6 M_{\odot} ; Kalirai et al. 2008), far above the $1.3 M_{\odot}$ turnoff of M67. This companion is therefore more compatible with an MS star. Another possibility could be that the system is a triple system composed of a near-turnoff primary star and a secondary that is a close binary composed of two low-mass stars ($\sim 0.5 M_{\odot}$). If these stars were spotted and tidally locked in a 2.3-day orbit, this could also explain the origin of the periodic signal. However, we note that some known WD-MS binaries do not fall on the expected Rappaport et al. (1995) relation (e.g., Kawahara et al. 2018; Gosnell et al. 2019). On their own, the secondary masses cannot definitely confirm or rule out the existence of WD companions for these sources.

5.4. UV Excesses Indicative of White Dwarf Companions

To look for evidence of companions to our systems, we examine their SEDs. We include UV photometry from *GALEX* (Martin et al. 2005), IR photometry from 2MASS (Skrutskie et al. 2007) and *WISE* (Wright et al. 2010), and optical photometry from Geller et al. (2015), originally obtained by Montgomery et al. (1993). Our SED fitting routine is described in Leiner et al. (2016). Briefly, we fit a grid of Castelli & Kurucz (2004) models of varying temperature and radius using χ^2 minimization. We fix the surface gravity to a typical MS value (log g=4.0), assume solar-metallicity models, and fix the reddening to the cluster value (E(B-V)=0.041;

Taylor 2007). We note that the SED fits are not particularly sensitive to our choice for surface gravity, metallicity, or reddening within a range of reasonable values. We set the distance to 850 pc, the median of the 800–900 pc range found for M67 in the literature (Geller et al. 2015).

We fit SEDs to these stars in three steps: (1) we fit a single, MS model; (2) we fit a combination of two MS stars; and (3) we fit the flux excluding the *GALEX* FUV photometry, as this is the only bandpass that would have substantial flux from a hot WD companion. If the best fit comes from method 1, we characterize the star as being single or having a low-luminosity companion. If the best fit comes from method 2, the system has a relatively bright MS secondary. If the best fit comes from method 3, this is indicative of a UV excess not well described by any MS companion. These stars may have hot WD companions contributing to their UV flux, or may have UV flux enhancements due to stellar activity. We show the best-fitting model for each star in our sample in Figure 7.

We find that the UV flux of WOCS 2068 can be well described by a combination of two stars (Figure 7(e))—one beginning to turn off the MS, and the other a BSS of \sim 6800 K. This SED fit is consistent with our interpretation of the photometric variability, in particular that the system combines a rapidly rotating merger or collision product (the 6800 K BSS) and a typical MS star.

Several other binaries in our sample also have UV excesses over single-star models that are not resolved by adding an MS companion. These include WOCS 14020, 12020, 3001, 6025, and 11006 (Figures 7(b), (c), (d), (g), and (h)).

WOCS 14020 is the only system where we consider this UV excess a definitive WD detection. Assuming a typical $0.5 \, M_{\odot}$ C/O WD model, the UV excess is most compatible with a $\sim 13,000$ K WD companion corresponding to an age of ~ 300 Myr (Tremblay et al. 2011).

For the rest of the binaries it is not clear whether their UV excesses indicate WD companions. All are hotter than WOCS 14020, making it more likely that the wide GALEX FUV passband picks up some flux from the Wien tail of the primary. Due to the low GALEX resolution and uncertainties on the spectral models in the UV, the uncertainties on predicted UV flux from the primary stars are large. In addition, these stars may have elevated UV fluxes owing to chromospheric emission, which might be expected given that they are all rapidly rotating. Similar excesses have been discovered in other FGK field stars using GALEX photometry that have been largely attributed to UV emission from stellar activity (Smith et al. 2014). The UV excesses are nevertheless large enough to be intriguing. While none of the fluxes are large enough to indicate a very young WD (<150 Myr), they could be compatible with cooler WD companions with ages of ≥150 Myr. We suggest follow-up observations using more precise, multiband UV photometry (e.g., HST/WFC3 as in Gosnell et al. 2015) to more definitively address the presence of WD companions.

Given the temperatures of the primaries and the *GALEX* detection limits, we might expect to detect WD companions hotter than \sim 13,000 K as UV excesses in the stellar SEDs, corresponding to an age younger than about 300 Myr. Notably, we detect UV excesses only in the binaries with the youngest rotational ages in our sample, all less than 300–400 Myr (Figure 1). The binary systems with older inferred gyro-ages (WOCS 4001, WOCS 9005) do not have UV detections (Figures 7(a), (f)). The gyro-ages and

UV excesses are therefore both compatible with the hypothesis that WOCS 4001 and WOCS 9005 formed earlier, and therefore now have cooler undetectable WD companions, and the other binaries formed recently enough to have hot, detectable WD companions.

Finally, only one of the single stars, WOCS 1020, has a *GALEX* FUV detection (Figure 7(i)). The others, WOCS 7035 and WOCS 2001, do not have FUV detections (Figures 7(j), (k)). The nondetection of these stars is as expected, as only WOCS 1020 is hot enough to expect FUV flux above the *GALEX* detection limit. SEDS of all three stars are fit best with a single-star MS model.

6. Summary and Discussion

Based on the findings of Leiner et al. (2018), we presume that mass transfer spins stars up to large rotational velocities at formation, and then these stars spin down as they age approximately as predicted by models for standard solar-type stars. As a result, a mass transfer event restarts a star's gyro-age clock. Models and observations of other BSS formation mechanisms (mergers and collisions) also likely yield rapidly rotating stellar products, though their spin-down behavior has not been empirically determined. Thus, it is not yet established that rotation rate is a reliable measure of time since formation for merger and collision products.

This spin-up at formation enables identification of BSS analogs within the MS by looking for stars in old populations with fast rotation rates. We pilot the use of this technique in M67 by measuring stellar rotation periods from K2 Campaigns 5 and 16 light curves, as well as from the spectral database of the WIYN Open Cluster Study. We find 11 rapid rotators on the M67 MS, all with rotation periods less than 8 days. None of these stars have close binary companions, so the rapid rotation is not due to tidal spin-up. We hypothesize that these stars have been through mass transfer, mergers, or stellar collisions within the past 1 Gyr.

These 11 detections have much in common with the BSS populations of old open clusters, including a binary fraction three times higher than the MS spectroscopic binary fraction of M67; a preponderance of long-period, low-eccentricity binary systems; and in at least one case a UV excess indicative of a young WD companion. These results suggest that these 11 sources are mass transfer, merger, or collision products and thus represent a low-luminosity extension of the BSS distribution. Given this hypothesis, we suggest calling this population of MS BSSs "blue lurkers," as they have been rejuvenated by mass transfer/mergers like the BSSs but blend with the normal MS population in the CMD. Presumably as the cluster ages, similar-mass stars will begin to evolve away from the MS, revealing these lurkers as the BSSs they truly are.

Because these stars cannot be detected as BSSs from their CMD location, this hidden population has not been characterized until now. With 11 detections, these blue lurkers are nearly as numerous as the classical BSS population of the cluster. This result suggests that population studies that focus only on classical BSSs are missing as much as half of the mass transfer, merger, and collision population.

These 11 blue lurker detections were selected from a sample of \sim 400 solar-type MS cluster members. Thus, at least 3% of normal MS stars are actually blue lurkers. In more detail, this sample includes 98 spectroscopic binaries ($P_{\rm orb} < 10^4$ days; Geller et al. 2015; A. M. Geller et al. 2019, in preparation). Eight of our 11 detections are among these binaries, implying

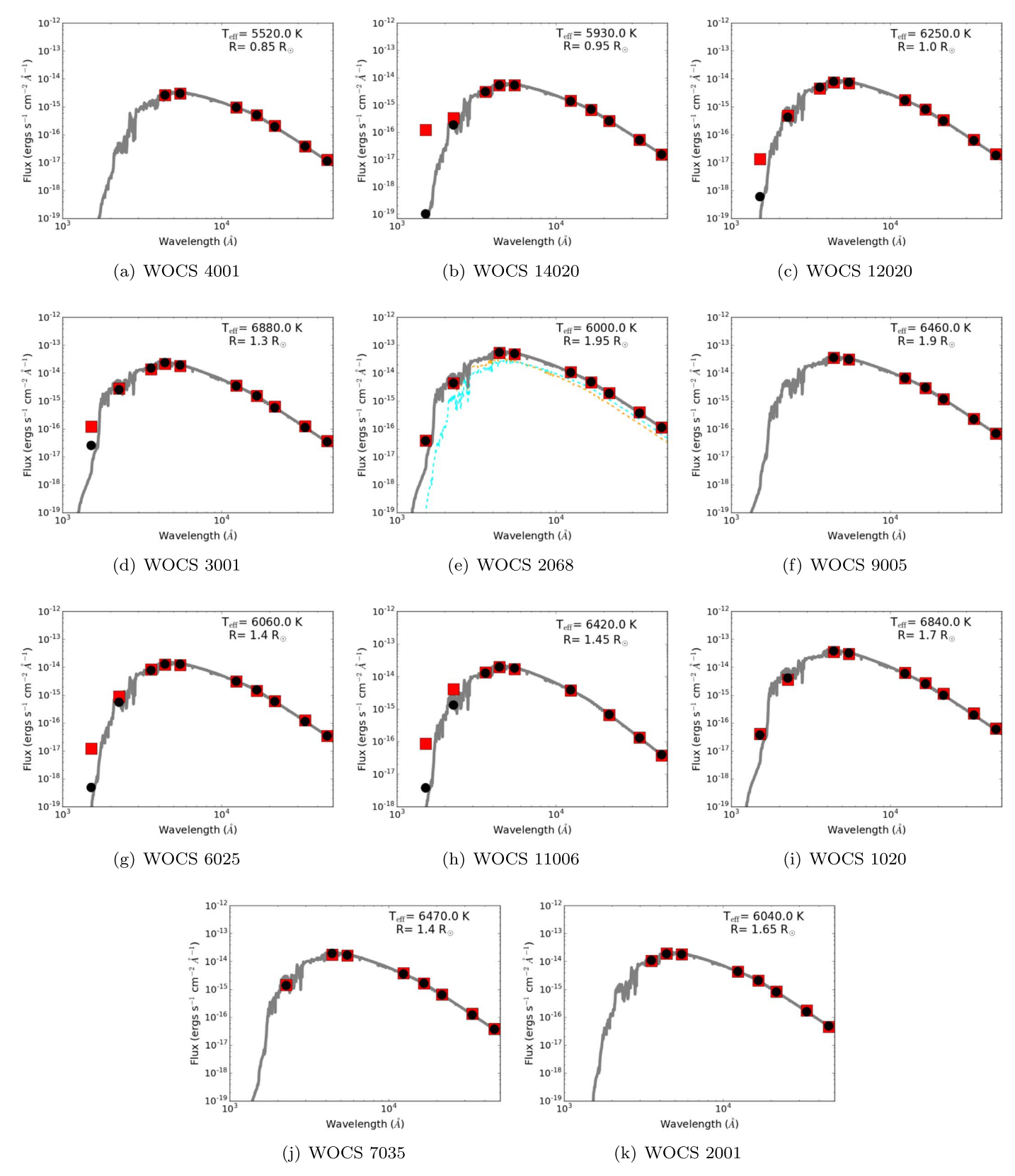


Figure 7. SEDs of the 11 rapid rotators in M67. We show the best-fit Castelli & Kurucz (2004) spectrum in gray. Black circles are synthetic observations created by convolving the spectrum with filter transmission functions for 2MASS, *WISE*, *GALEX*, and Johnson *UBV* filters. The real observations are shown with red squares. For one system, WOCS 2068, we use a two-star model. In this case we plot the primary model (6000 K, 1.95 R_{\odot}) in cyan, the secondary model (6800 K, 1.5 R_{\odot}) in orange, and the combined flux in black.

that at least 8% of the solar-type spectroscopic binary population consists of blue lurkers. Of these eight, we suggest that at least five are recent mass transfer products given their secondary masses (Figure 6), indicating that at least 5% of the solar-type spectroscopic binary population has been through mass transfer within the past 1 Gyr. Three systems are observed to be single stars, indicating that $\sim \! 1\%$ of the MS is composed of spun-up merger or collision products. If merger products spin down in much the same way as we have demonstrated for mass transfer products, these stars may also have formed within the past 1 Gyr.

This result is illustrative of the ways binary evolution can impact a stellar population. If 11 stellar systems in M67 have been through a stellar collision or mass transfer event in the past 1 Gyr, it is certain that other stars on the MS have also experienced stellar interactions in the more distant past and have since spun down. Indeed, 4 of the 11 blue lurkers in our sample are near the zero-age MS (Figure 2). Such stars likely result from mass transfer onto lower-mass, largely unevolved stars and themselves will live for several 1 Gyr before evolving off the MS.

Older blue lurker systems would likely show up with intermediate rotation periods (i.e., 8-15 days). These slower rotators would be less magnetically active with smaller and shorter-lived spots, making them harder to identify through rotational modulation. Similarly, their slower rotation rates would make them undetectable using $v \sin i$ measurements in all but very high resolution spectroscopic studies. These slower rotation periods are also closer to typical cluster rotation rates, making these blue lurkers more difficult to distinguish from typical M67 single stars. Such stars may nevertheless contribute to the spread of rotation rates observed in the cluster, skewing measurements toward shorter rotation periods and complicating efforts to calibrate precise gyrochronology relationships in clusters.

As a simple upper bound, if we suppose that formation rates of FGK-type blue lurkers remained constant over the 4 Gyr history of the cluster, this implies that up to $\sim 30\%$ of solar-type binaries and $\sim 4\%$ of the single MS stars have been through an interaction during their lifetimes. Though a very simple estimate, these numbers are in rough agreement with other studies. Andronov et al. (2006) predict that 3%–4% of MS stars in M67 may be merger products. Murphy et al. (2018) find that $\sim 20\%$ of the field A/F-type binaries within a similar period range are post-mass-transfer binaries. The post-interaction fraction among older binary populations is sizable.

Several other clusters have the *K*2 and *Kepler* light curves needed to detect blue lurker populations, including NGC 6791, NGC 6819, and Ruprecht 147. Studies of additional clusters such as these, combined with detailed binary population modeling, will be required to quantify more precisely what the impact of binary interactions may be on the rotational properties of cluster stellar populations.

The full population of blue lurkers on cluster MSs remains largely unexplored because of the difficulties in detecting them. As a result, the stellar and orbital properties of this significant population have not been well characterized. Already there are hints that this population may yield new insights into binary evolution physics. For example, three stars in our sample have orbital periods of just 100–400 days, shorter periods than almost all BSSs, and an orbital period domain thought to be sparsely populated with MS–WD binaries (e.g., Willems & Kolb 2004).

For the two faintest systems, the inferred mass ratios $(\frac{M_{\text{donor}}}{M_{\text{accretog}}})$ at the onset of mass transfer strongly predict unstable mass transfer (e.g., Chen & Han 2008), yet they have survived without the dramatic orbital shrinkage expected during common-envelope evolution. Building a larger sample of post-mass-transfer blue lurkers across more clusters is necessary to see whether these types of orbits are indeed common among the class. Future detailed evolutionary modeling will also be required to better understand possible formation pathways.

Kepler and K2 have opened the door to detecting lowerluminosity mass transfer, merger, and collision products on the MS using rotation rates. With similar future missions like TESS and PLATO planned for the near and longer-term future, rotational studies of stars in clusters and in the field will continue to be important areas of study. TESS will yield rotation periods for nearby stars in younger clusters (<1 Gyr) and the field. Looking for rapidly rotating field stars with abundances or kinematics indicative of old age may be a viable detection method for field post-mass-transfer binaries. Due to the large scatter in rotation rates among young stars, this technique may not be well suited to identifying interaction products in TESS clusters. If PLATO, planned for launch in 2026, targets more older clusters, more rotational identifications of blue lurkers may be possible. As the known population continues to grow, these populations can provide new tests for binary evolution physics and cluster population models.

E.L. is supported by an NSF Astronomy and Astrophysics Postdoctoral Fellowship under award AST-1801937. R.D.M. acknowledges funding support from NSF AST-1714506 and NASA-NNX15AW69G. A.V.'s work was performed under contract with the California Institute of Technology (Caltech)/ Jet Propulsion Laboratory (JPL) funded by NASA through the Sagan Fellowship Program executed by the NASA Exoplanet Science Institute. Thank you to R. Esselstein for helpful conversations about stellar rotation periods for this paper. Thank you also to the anonymous referee for careful and thoughtful comments on the manuscript.

ORCID iDs

Emily Leiner https://orcid.org/0000-0002-3944-8406
Robert D. Mathieu https://orcid.org/0000-0002-7130-2757
Andrew Vanderburg https://orcid.org/0000-0001-7246-5438
Natalie M. Gosnell https://orcid.org/0000-0002-8443-0723
Jeffrey C. Smith https://orcid.org/0000-0002-6148-7903

References

Aigrain, S., Hodgkin, S. T., Irwin, M. J., Lewis, J. R., & Roberts, S. J. 2015, MNRAS, 447, 2880
Almenara, J. M., Alonso, R., Rabus, M., et al. 2012, MNRAS, 420, 3017
Andronov, N., Pinsonneault, M. H., & Terndrup, D. M. 2006, ApJ, 646, 1160
Angus, R., Aigrain, S., Foreman-Mackey, D., & McQuillan, A. 2015, MNRAS, 450, 1787

Aoki, W., Beers, T. C., Sivarini, T., et al. 2008, ApJ, 678, 1351

Balona, L. A. 2018, MNRAS, 479, 183

Balona, L. A., & Abedigamba, O. P. 2016, MNRAS, 461, 497

Balona, L. A., Guzik, J. A., Uytterhoeven, K., et al. 2011, MNRAS, 415, 3531 Barnes, S. A. 2003, ApJ, 586, 464

Barnes, S. A., Weingrill, J., Fritzewski, D., Strassmeier, K. G., & Platais, I.

Bressan, A., Marigo, P., Girardi, L., et al. 2012, MNRAS, 427, 127

Breton, R. P., Rappaport, S. A., van Kerkwijk, M. H., & Carter, J. A. 2012, ApJ, 748, 115

```
Carney, B. W., Latham, D. W., Laird, J. B., Grant, C. E., & Morse, J. A. 2001,
   AJ, 122, 3419
Carney, B. W., Lee, J.-W., & Dodson, B. 2005, AJ, 129, 656
Castelli, F., & Kurucz, R. L. 2004, arXiv:astro-ph/0405087
Chen, X., & Han, Z. 2008, MNRAS, 387, 1416
Corsaro, E., Stello, D., Huber, D., et al. 2012, ApJ, 757, 190
de Mink, S. E., Langer, N., Izzard, R. G., Sana, H., & de Koter, A. 2013, ApJ,
Epstein, C. R., & Pinsonneault, M. H. 2014, ApJ, 780, 159
Esselstein, R., Aigrain, S., Vanderburg, A., et al. 2018, ApJ, 859, 167
Fan, X., Burstein, D., Chen, J.-S., et al. 1996, AJ, 112, 628
Fornasini, F. M., Tomsick, J. A., Bodaghee, A., et al. 2014, ApJ, 796, 105
Fregeau, J. M., Cheung, P., Portegies Zwart, S. F., & Rasio, F. A. 2004,
    MNRAS, 352, 1
Gallet, F., & Bouvier, J. 2013, A&A, 556, A36
Gallet, F., & Bouvier, J. 2015, A&A, 577, A98
Geller, A. M., Hurley, J. R., & Mathieu, R. D. 2013, AJ, 145, 8
Geller, A. M., Latham, D. W., & Mathieu, R. D. 2015, AJ, 150, 97
Geller, A. M., Mathieu, R. D., Harris, H. C., & McClure, R. D. 2008, AJ,
   135, 2264
Geller, A. M., Mathieu, R. D., Harris, H. C., & McClure, R. D. 2009, AJ,
   137, 3743
Girard, T. M., Grundy, W. M., Lopez, C. E., & van Altena, W. F. 1989, AJ, 98, 227
Gonzalez, G. 2016, MNRAS, 463, 3513
Gosnell, N. M., Leiner, E. M., Mathieu, R. D., et al. 2019, arXiv:1904.02280
Gosnell, N. M., Mathieu, R. D., Geller, A. M., et al. 2014, ApJL, 783, L8
Gosnell, N. M., Mathieu, R. D., Geller, A. M., et al. 2015, ApJ, 814, 163
Handberg, R., Brogaard, K., Miglio, A., et al. 2017, MNRAS, 472, 979
Handler, G. 1999, MNRAS, 309, L19
Hansen, T. T., Andersen, J., Nordström, B., et al. 2016, A&A, 588, A3
Hartman, J. D., Gaudi, B. S., Holman, M. J., et al. 2008, ApJ, 675, 1254
Ivanova, N., Heinke, C. O., Rasio, F. A., Belczynski, K., & Fregeau, J. M.
   2008, MNRAS, 386, 553
Jeffries, R. D., & Stevens, I. R. 1996, MNRAS, 279, 180
Jorissen, A., Van Eck, S., Mayor, M., & Udry, S. 1998, A&A, 332, 877
Jorissen, A., Van Eck, S., Van Winckel, H., et al. 2016, A&A, 586, A158
Kalirai, J. S., Hansen, B. M. S., Kelson, D. D., et al. 2008, ApJ, 676, 594
Kawahara, H., Masuda, K., MacLeod, M., et al. 2018, AJ, 155, 144
Kaye, A. B., Handler, G., Krisciunas, K., Poretti, E., & Zerbi, F. M. 1999,
     ASP, 111, 840
Landsman, W., Aparicio, J., Bergeron, P., Di Stefano, R., & Stecher, T. P.
   1997, ApJL, 481, L93
Leigh, N., & Sills, A. 2011, MNRAS, 410, 2370
Leiner, E., Mathieu, R. D., Gosnell, N. M., & Sills, A. 2018, ApJL, 869, L29
Leiner, E., Mathieu, R. D., Stello, D., Vanderburg, A., & Sandquist, E. 2016,
    ApJL, 832, L13
Leonard, P. J. T. 1989, AJ, 98, 217
Li, L., Zhang, F., Han, Q., Kong, X., & Gong, X. 2014, MNRAS, 445, 1331
Lovisi, L., Mucciarelli, A., & Ferraro, F. R. 2010, ApJL, 719, L121
Lurie, J. C., Vyhmeister, K., Hawley, S. L., et al. 2017, AJ, 154, 250
Martin, D. C., Fanson, J., Schminovich, D., et al. 2005, ApJL, 619, L1
Mathieu, R. D. 2000, in ASP Conf. Ser. 198, Stellar Clusters and Associations:
   Convection, Rotation, and Dynamos, ed. R. Pallavicini, G. Micela, &
   S. Sciortino (San Francisco, CA: ASP), 517
Mathieu, R. D., & Geller, A. M. 2009, Natur, 462, 1032
```

```
Mathieu, R. D., van den Berg, M., Torres, G., et al. 2003, AJ, 125, 246
Matt, S., & Pudritz, R. E. 2005, MNRAS, 356, 167
McCrea, W. H. 1964, MNRAS, 128, 147
Meibom, S., Barnes, S. A., Platais, I., et al. 2015, Natur, 517, 589
Meibom, S., Grundahl, F., Clausen, J. V., et al. 2009, AJ, 137, 5086
Meibom, S., & Mathieu, R. D. 2005, ApJ, 620, 970
Meibom, S., Mathieu, R. D., & Stassun, K. G. 2006, ApJ, 653, 621
Milliman, K. E., Leiner, E., Mathieu, R. D., Tofflemire, B. M., & Platais, I.
  2016, AJ, 151, 152
Milliman, K. E., Mathieu, R. D., Geller, A. M., et al. 2014, AJ, 148, 38
Montgomery, K. A., Marschall, L. A., & Janes, K. A. 1993, AJ, 106, 181
Mucciarelli, A., Lovisi, L., Ferraro, F. R., et al. 2014, ApJ, 797, 43
Murphy, S. J., Moe, M., Kurtz, D. W., et al. 2018, MNRAS, 474, 4322
Naoz, S., & Fabrycky, D. C. 2014, ApJ, 793, 137
Nemec, J. M., Balona, L. A., Murphy, S. J., Kinemuchi, K., & Jeon, Y.-B.
  2017, MNRAS, 466, 1290
Nissen, P. E., Twarog, B. A., & Crawford, D. L. 1987, AJ, 93, 634
Packet, W. 1981, A&A, 102, 17
Parsons, S. G., Agurto-Gangas, C., Gansicke, B. T., et al. 2015, MNRAS,
  449, 2194
Parsons, S. G., Rebassa-Mansergas, A., Schreiber, M. R., et al. 2016, MNRAS,
  463, 2125
Perets, H. B., & Fabrycky, D. C. 2009, ApJ, 697, 1048
Phinney, E. S., & Sigurdsson, S. 1991, Natur, 349, 220
Raghavan, D., McAlister, H. A., Henry, T. J., et al. 2010, ApJS, 190, 1
Rappaport, S., Podsiadlowski, P., Joss, P. C., Di Stefano, R., & Han, Z. 1995,
      IRAS, 273, 731
Rebassa-Mansergas, A., Gänsicke, B. T., Schreiber, M. R., Koester, D., &
  Rodríguez-Gil, P. 2010, MNRAS, 402, 620
Rebassa-Mansergas, A., Ren, J. J., Irawati, P., et al. 2017, MNRAS, 472, 4193
Rebull, L. M., Stauffer, J. R., Bouvier, J., et al. 2016, AJ, 152, 114
Reinhold, T., & Gizon, L. 2015, A&A, 583, A65
Sanders, W. L. 1977, A&AS, 27, 89
Sarajedini, A., Dotter, A., & Kirkpatrick, A. 2009, ApJ, 698, 1872
Shetrone, M. D., & Sandquist, E. L. 2000, AJ, 120, 1913
Sills, A., Adams, T., & Davies, M. B. 2005, MNRAS, 358, 716
Sills, A., Adams, T., Davies, M. B., & Bate, M. R. 2002, MNRAS, 332, 49
Sills, A., Faber, J. A., Lombardi, J. C., Jr., Rasio, F. A., & Warren, A. R. 2001,
    ApJ, 548, 323
Skrutskie, M. F., Cutri, R. M., & Marsh, K. A. 2007, BAAS, 39, 836
Smith, J. C., Stumpe, M. C., Van Cleve, J. E., et al. 2012, PASP, 124, 1000
Smith, M. A., Bianchi, L., & Shiao, B. 2014, AJ, 147, 159
Stello, D., Vanderburg, A., Casagrande, L., et al. 2016, ApJ, 832, 133
Strope, R. J., Schaefer, B. E., & Henden, A. A. 2010, AJ, 140, 34
Stumpe, M. C., Smith, J. C., Catanzarite, J. H., et al. 2014, PASP, 126, 100
Szkody, P., Anderson, S. F., Brooks, K., et al. 2011, AJ, 142, 181
Taylor, B. J. 2007, AJ, 133, 370
Tremblay, P.-E., Bergeron, P., & Gianninas, A. 2011, ApJ, 730, 128
van den Berg, M., Tagliaferri, G., Belloni, T., & Verbunt, F. 2004, A&A,
  418, 509
van Roestel, J., Kupfer, T., Ruiz-Carmona, R., et al. 2018, MNRAS, 475, 2560
Vanderburg, A., & Johnson, J. A. 2014, PASP, 126, 948
Vanderburg, A., Latham, D. W., Bucchave, L. A., et al. 2016, ApJS, 222, 14
Willems, B., & Kolb, U. 2004, A&A, 419, 1057
Wright, E. L., Eisdenhardt, P. R. M., Mainzer, A. K., et al. 2010, AJ, 140, 1868
```